PERFORMANCE EVALUATION OF TRACER PARTICLES FOR PARTICLE IMAGE VELOCIMETRY USING A SCALED ROLLING ROAD-TIRE SETUP IN A WIND TUNNEL

by

Nithin Narayan

A thesis submitted to the faculty of
The University of North Carolina at Charlotte
in partial fulfillment of the requirements
for the degree of Master of Science in
Applied Energy and Electromechanical Systems

Charlotte

2018

Approved by:

_____

Dr. Navid Goudarzi

_____

Dr. Peter Tkacik

_____

Dr. Rodward L Hewlin Jr.

ABSTRACT

NITHIN NARAYAN. Performance Evaluation of Tracer Particles for Particle Image Velocimetry Using a Scaled Rolling Road-Tire Setup in a Wind Tunnel. (Under the direction of DR. NAVID GOUDARZI)

The ultimate goal of the present work is to evaluate the ability to produce highly resolved particle image velocimetry (PIV) flow images of tracer particles dispersed in a wind tunnel with a scaled rolling road-tire setup. The particle type, size, and density impact the instantaneous velocity profile measurement uncertainty. Three types of tracer particles including smoke, olive oil, and helium filled soap bubbles (HFSB) were used in this study. The experimental setup consist of a 1/10th scaled slick tire on a rolling road in a 0.3 m^3 test section of an open-return eiffel wind tunnel with a free stream velocity of 11 m/s. For PIV analyses in the present work, a dual power Nd:YAG laser in conjunction with a sCMOS camera was used to provide a laser light sheet to illuminate particles and obtain time resolved images of the flow field in the test section. A commercial PIV software was used to analyze images and detect vortex formation. The experiments were conducted initially without a prototype in the wind tunnel; i.e. empty tunnel testing and then with the tire inserted into the test section. It was found that the HFSB seeding was not providing a consistent density throughout the test section. Comparing the olive oil and smoke for scaled tire testing, it was found that the olive oil yielded higher resolution images as compared to the smoke tracer particles. Hence, the tests on the case study were conducted using olive oil and smoke. An analogous behavior obtained from the empty channel testing for two seeding particles was observed in conducted tests on the case study.

ACKNOWLEDGEMENTS

I would like to thank my advisor Dr. Navid Goudarzi for giving me the opportunity to do this research and his support throughout the entirety of this research. I would also like to thank Dr. Peter Tkacik and Dr. Rodward Hewlin for their valuable inputs and guidance regarding the research and for serving on my thesis committee. I would like to especially thank Dr. Jerry Dahlberg, Stuart Gambill and Tucker Bisel for their technical expertise, friendship and their helpful guidance throughout this research.

I would also like to thank my family for allowing me to pursue my Masters and my friends for supporting me through the tough times.

DEDICATION

To my little brother

Niketh Narayan (1995-2013)

TABLE OF CONTENTS

LIST OF FIGURES

LIST OF ABBREVIATIONS

HFSB Helium Filled Soap Bubbles

LDA Laser Doppler Anemometry

PIV Particle Image Velocimetry

CHAPTER 1: INTRODUCTION

Particle Image Velocimetry is a non-intrusive technique which uses tracer particles which are dispersed into flow medium to study flow visualization. The tracking ability of the particles are important so as to obtain accurate results. For most of the studies, generally, tracer particles are selected from a list of compatible seedings based on the previous experimentation setup available in literature. The are not many studies which focus on comparing different tracer particles for an experimental study and their impact on the results. For this work, a case study is presented on flow visualization over a scaled tire on a rolling road. Airflow over a tire is selected so as to study drag and thus, impacts the overall fuel efficiency for a vehicle. In this thesis a comparison of tracer particles is made using multiple tracer particles with a rolling road-tire setup as a case study. The flow around a tire on a rolling road is done so as to The vortex formation around the tire is set as the baseline for comparison for different types of tracer particle seedings. This case study was selected so as to facilitate a moving test section and as a precursor for further experimentation with the same setup or similar setup.

In Chapter 2, a general background on tracer particles and the case study is presented. This chapter gives a background about the characteristics for the selection of tracer particles and also on the works which deals with the case study being conducted.

Chapter 3 gives more insight into the principles of Particle Image Velocimetry, the methods of production and distribution of olive oil, Smoke and HFSB as tracer particles inside the wind tunnel.Chapter 2 also focuses on the open return wind tunnel and the modifications done to it, the rolling road-tire setup, the settling chamber and

the specifications of the camera and the laser. This chapter also talks about the empty channel and rolling road-tire calibration, testing and processing.

Chapter 3 discusses the results obtained from the empty channel testing and the rolling road-tire setup testing using the tracer particles and a comparison of flow visualization results is done between the tracer particles.

Chapter 4 discusses the conclusions and challenges encountered in this study.

CHAPTER 2: GENERAL BACKGROUND

In PIV, the flow is visualized by distributing a suspension of tracer particles into the flow medium. The tracer particles are illuminated by a laser pulses within a short time interval. This helps to find the velocity at the test section being studied. The accuracy of the PIV results depends on several factors out of which the characteristics, generation, dispersion and scattering of these tracer particles play an important role. The tracer particles which are being dispersed into the flow should have matching densities to that of the flow medium being investigated i.e. the tracer particles should be neutrally buoyant. If the external forces like gravitational, centrifugal and electrostatic can be considered negligible, then the tracking ability of a tracer particle is governed by a factor called settling velocity. This settling velocity is derived from the Stokes drag law as described in [1, 2]

$$u_\infty = \frac{g d_p^2 (\rho_p - \rho_f)}{18\mu} \tag{2.1}$$

where u_∞ is the settling velocity, ρ_p is the tracer particle density, ρ_f is the fluid density, μ is the fluid viscosity, d_p is the diameter of tracer particle, g is the acceleration due to gravity. The best tracer particles are the ones where the settling velocity u_∞ is minimal.

The scattering characteristics of a tracer particle determines the intensity and the contrast of the image obtained by the camera sensor. The scattering of the tracer particles depends on the the ratio of refractive indices between the particle and the medium, particle size, shape, and orientation. A good documentation of light scattering theory is given by Melling [1]. It is stated that the scattering capability C_s

or the scattering cross section is a function of ratio of total scattered power to the incident light intensity. The total scattered power depends on the diameter and the incident light intensity depends on the wavelength.

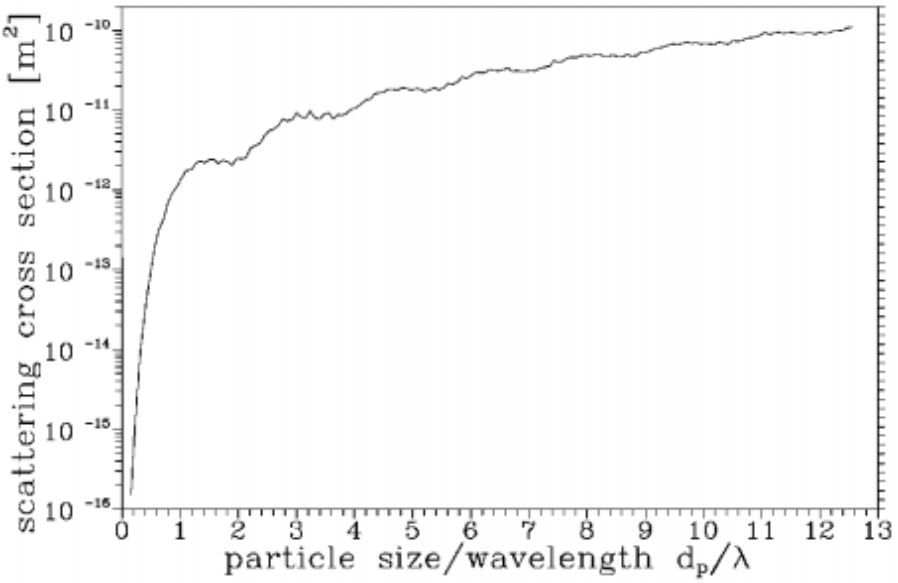

Figure 2.1: The scattering cross section as a function of the particle size (refractive index m=1.6) obtained from the work of Melling (1997) [1]

The figure 2.1 gives a the scattering capability as a function of the ratio of particle diameter d_p to the laser wavelength λ for spherical particles. From the figure 2.1, it can be concluded that the particle diameter should not be so small so as it affects the scattering efficiency.

For liquid flow seedings, the consequences of particles with slight mismatch in densities are not severe and the liquid flows are usually seeded with solid particles which recirculate in a closed loop water tunnel. Most of the tracer particles used will have a density within a few percent of the density of water The size of particles does not usually fluctuate after suspension. For the case of gaseous seeding , the commonly used tracer particles are oil or other solid particles. For gaseous flows, due to the large density difference between the tracer particles and the gaseous medium, to minimize the settling velocity, the diameter of the particle should be reduced. However, the

particle size dispersed should also be able to scatter the laser light so as to sufficiently illuminate the test section for imaging. Thus a compromise between accurate tracking and scattering should be found so as to determine the size of the tracer particles used for gaseous medium experimentation for PIV. For gaseous flows, the seeding of the test section causes some complications. The complications of the gaseous seeding are highlighted in the early works in literature by [3, 4, 5, 6, 7]. These papers describe the difficulties in getting consistent seeding and accurately tracking the gaseous flow tracer particles for high speed PIV experimentation.

For this current experimental study, an analysis is done to find how different tracer particles perform in gas flows in a small-scale wind tunnel setup using PIV with rolling road-tire as a case study. For wind tunnel experimentation, there are several methods of seeding the flow. Gas flows are typically seeded with either liquid droplets or solid particles. Seeding generators are used to produce the tracer particles. The seeding generators must produce uniformly sized tracer particles and at a high enough rate so as to get a good spatial resolution of PIV test section. According to Keane and Adrian [8], the number of particles required per interrogation volume should be around 15 particles. The works of Hunter and Nichols[9] , Kahler and Sammler[10], Kahler[11] and Melling[12] highlight some of the earliest seeding techniques used for gas flow experimentation. Seeding with liquid tracer particles is beneficial because:

1. Uniform production rate when compared to solid particles.

2. Inherent spherical shape of the particles is an advantage for assessing scattering characteristics and tracking behavior.

3. Readily available information about the densities of liquid tracer particles when compared to that of solids.

Solid particles are preferred when high particle concentrations are necessary. For the present work, solid particles are avoided because the study is done in an open return wind tunnel. It will be difficult to maintain a uniform solid particle seeding inside the

wind tunnel. It is also ill-advised to use solid particles for open return wind tunnels because of health concerns and more cost associated with increasing seeding. For these reasons, the experimental study was done with liquid droplets as tracer particles as these particles can produce consistent seeding for open return wind tunnel and are non-toxic. The study was done with olive oil, Smoke and HFSB as tracer particles. For liquid droplet seeding for gas flows, the generation of the droplets is done by atomization so as to generate particles of small size for PIV experimentation.

A comparison of tracer particles was done with a rolling road tire setup built in-house by [13] attached to a small-scale wind tunnel at the base of the test section as the case study. This case study was chosen for two reasons. The first reasoning is not to have a static test section i.e. to compare the tracer particles when the scaled model inside the test section is moving. This would add further complexity to the comparison. Secondly, so as to do future rolling road-tire experimentation with the setup at UNC Charlotte Motorsports Lab or a similar experimental setup.

For evaluating the case study, previous works done for rolling road-tire experimentation and the methods of seeding used will be reviewed A study of flow around a tire in contact with the ground is an important parameter in designing tires of commercial vehicles to reduce drag and improves overall fuel efficiency. For a tire study, it is difficult to incorporate a rolling road-tire setup i.e. a moving ground due to complications arising when a tire is in contact with a ground. The aerodynamic structures of the tire on a stationary ground are significantly different from that of a moving ground. These aerodynamic structures namely the vortices are dependent on the pressure differential around the tire and in turn also dependent on the lift and drag forces. To accurately depict the flow around a tire, a moving ground has to be taken into consideration which impacts the flow structures and the lift and drag forces around the tire. There are several works which highlight detailed experimental analysis of wake behind isolated tires for both stationary and rolling tires.

To understand the difficulties to model a tire on a moving ground setup, a look into works which try to model tire aerodynamics is presented so as get a better idea about it.

In order to understand the difficulties when trying to model a tire on a moving ground,

Early studies of the flow around a tire were carried out by Morelli [14], Stapleford and Carr [15] and Cogotti [16]. These studies were done on tires with non-moving ground inside the wind tunnel. A gap between the tire and the static ground was necessary to spin the tire so as to emulate a real world condition. It was found that when the gap was not sealed it produces a venturi effect, which accelerated the air underneath the tire causing a low pressure, thus producing negative lift.

It was also observed that when the gap was sealed as in the studies done by Stapleford and Carr and Cogotti, then the tire produced a positive lift. Thus, the removal of this gap was a significant in the early developmental studies on tires. This was done with the help of a moving ground, thus closing the gap as well as creating a realistic rolling conditions for testing. For a stationary ground case the airflow entering the tunnel builds up a boundary layer and this build-up creates a non-uniform velocity profile at the surface of the tire, most importantly at the contact patch. By using a moving ground allows for a uniform velocity profile for the boundary layer over the tire.

The work of Fackrell [17] [18], is one of the most important advancements in the study of isolated wheel aerodynamics. In his study, the author investigated six different wheels with differing sidewall profiles in contact with the ground. He proposed the existence of a large pressure peak followed by a trough in the static pressure distribution around the tire boundary. The pressure distribution was obtained by using pressure taps inside of the tire. He was able to obtain pressure peak which he had postulated. Fackrell concluded that high pressure peak is caused by the vis-

cous effect created by the intersecting shear layers at the frontal contact patch. This phenomenon is named as Fackrell's jetting phenomenon.

Axon et.al [19] also observed a strong jetting effect for a wheel in a wheel housing therefore concluded that the presence of jetting phenomenon is independent of tire geometry. The results from the study also aligned with the expected results from the literature.This study done by Fackrell is important because this formed as a baseline for further tire aerodynamic studies. This hypothesis was further confirmed in subsequent studies by Bearman [20] and Mercker and Berneburg[21]. Further, the negative pressure peak postulated by Fackrell was experimentally detected by [22] [23]. All of the above mentioned studies gave a good insight on how to setup the configuration for this study.

Several experimental works were done with the help of PIV and Laser Doppler Anemometry (LDA). These works are important to understand the vortex formation generated around the tire. This vortex formation is used as a reference for comparison in this study between the tracer particles. Waschle [24] performed an experimental analysis on deformable tire. The flow visualization was done with 3-D LDA system. Waschle validated their earlier CFD simulation and not the entire flow field itself. There was a strong down-wash obtained from a stationary case as seen in the study Mears [25].

Another study done by Saddington et al [26] conducted a study to generalize the flow field around a tire. The study was done by using LDA on 50 percent scaled tire. They were able to study the developing flow field of the rotating wheel. They concluded that the central region and ground vortices produce an inverted T-shape wake. Saddington reasoned that the asymmetric nature of the vortices might be due to the support sting and this was verified by Knowles [27]. Axerio et al [28]. studied the airflow around the tire and compared the experimental work with two CFD codes, LES and RANS. The experimental work is done by using PIV. They were able to show

that near wake of the tire is dominated by two large counter-rotating vortices similar to other experimental results. Their work also revealed a periodic oscillation of vortex centers. The work showed the sensitivity of turbulence models by comparing vortex core locations using RANS, LES with that of PIV. The locations of vortex cores in the fine LES method was found accurate with that of PIV analysis. The oscillation of these vortex core structures seems to be due to the interrogation methods or due to the deformable tire, but it needs further investigation.

AJ Sprot [29] in his work studied the impact of load on a deformable tire and the sensitivity of this load to the sidewall profile of the tire. They found that the sidewall was most sensitive to the axle height. Their work also found that the change in sidewall profile caused a significant change in the aerodynamic performance of the tire. Higher levels of sidewall deformation resulted in a larger wake structure and increased drag forces. Issakhanian [30] studied the wake behind an isolated tire using PIV measurements using a pneumatic, deformable tire loaded vertically to create the shoulder profiles and contact patch as well as using spoked wheel, brake cooling ducts. This setup is reminiscent of an actual brake assembly setup. The authors found out that the lower counter-rotating pairs of vortices are heavily affected by the brake cooling ducts. Mears et al [23] found the lift and drag forces using a load cell. The coefficients of lift and drag forces were measured to study the flow in the wake of the tire and to give a qualitative assessment of the counter-rotating vortex phenomenon.

All these studies came up with the same asymmetric wake profile as previous studies. These experimental studies gives a template to analyze the flow for the current experimentation and to understand the different vortices to be visualized. The current study focuses on studying these observed flow patterns by using a small scale, low-cost rolling road setup as mentioned in previous work of Tkacik et. al.[13]. Tkacik built a low cost rolling road using belt sander to facilitate for further experimentation at Motorsports Lab UNCC. A rolling road normally needs a lot of investment. This

experimental setup design would be able to eliminate the cost of rolling road from the further experimentation cost. This would drastically cut down the experimentation cost but would still produce comparable results to that of other studies.

From the literature, there are not many studies which qualitatively compare tracer particle performance for a particular experimentation. A paper by Hamdi.M [31] compared multiple tracer particles for use in his electrodydonamic study. The study made a comparison between SiO_2, TiO_2, Expancel Microspheres (EMS), incense or cigarette smoke and oil smoke. It was found that SiO_2, TiO_2 incense or cigarette smoke were rarely influenced by electric field, while the EMS particles and the oil smoke were greatly affected. There are no current studies which qualitatively compare different tracer particles for flow visualization over a tire.The current study attempts to find the best performing tracer particle for flow visualization with a rolling road-tire experimentation.

CHAPTER 3: EQUIPMENTS AND METHODS

3.1 Particle Image Velocimetry

PIV provides information regarding the magnitude and direction of the velocity of the flow field. The velocity information is obtained from the seeding particles dispersed in the flow and is based on the displacement of these particles over a known time interval. From this displacement, velocity information can be extracted. Unlike other flow measurement methods like LDA or the five-hole pressure probe, for a PIV an entire image plane is captured to reveal the nature of flow in that plane.

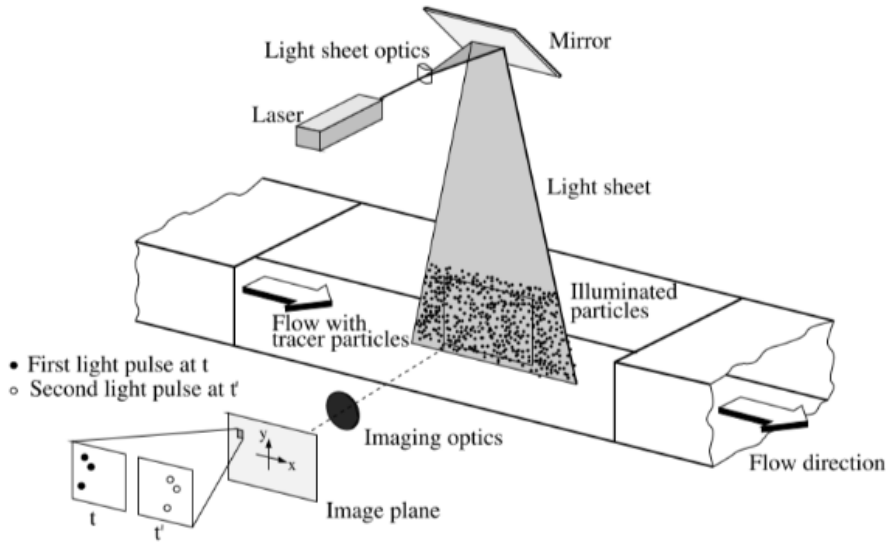

Figure 3.1: General experimental setup for PIV as represented, Raffel[32]

The laser with the help of optics produces a light sheet. The light sheet is captured by a high-speed sCMOS camera. A synchronizer is used to synchronize the timing of laser pulse with that of the camera trigger thus ensuring that the camera is able to capture all the information from light sheet created by the pulsing laser. The airflow is seeded with neutrally buoyant particles which are entrained in the fluid flow and

these particles are illuminated by the laser and are captured by the imaging system of the camera. The tracer or seeding particle is created by smoke generator and an olive oil atomizer which produces particles roughly 1 micrometer in diameter. The images are then processed via cross-correlation and raw velocity vector maps are produced.

3.2 Wind Tunnel and Rolling Road-Tire Mount Setup

Figure 3.2: Wind tunnel with settling chamber

The wind tunnel situated at Motorsports Research Lab at UNC Charlotte is a low speed open return Eiffel wind tunnel with a test section of $0.3m^2$. In recent years, several modifications have been done to the wind tunnel. The modifications are done so that the wind tunnel is flexible for variety of experimentation. The modifications done on the tunnel include replacing the opaque wooden walls of the wind tunnel by Lexan ®sheets so as to be able to visualize the model which is mandatory in case of Particle Image Velocimetry studies. The Lexan ®sheets covering the test section are made modular so as to have an easy access to the test section to make quick changes to the experimental setup [33]

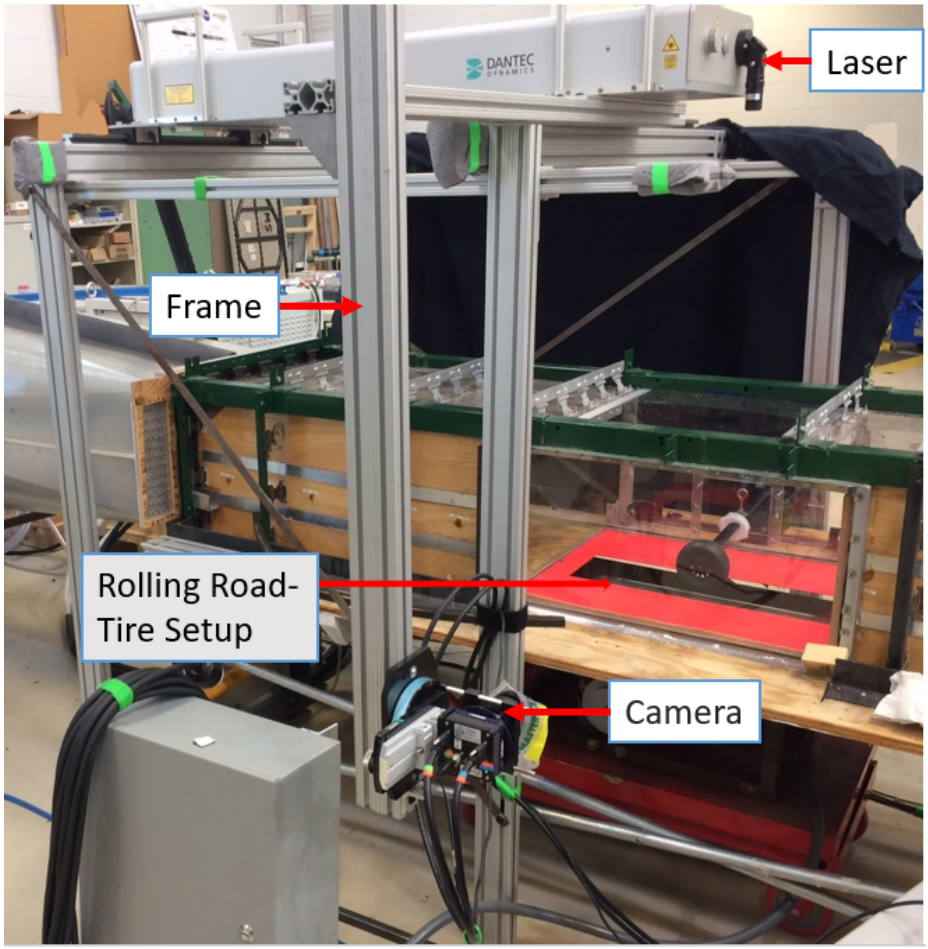

Figure 3.3: Experimental setup for rolling road-tire testing. Image credits: [33].

Further, the base of the tunnel was retrofitted with the rolling road built in-house by modifying a belt sander as mentioned in the work of Tkacik et al. [13]. For this experimental study, the belt sander body was removed and replaced with iron tubings so as to fit this setup underneath the base of the wind tunnel as shown in the fig 3.3.

For the tire mount a 1/10th scale tire was used. This tire was attached to a makeshift stinger made using an airfoil. The stinger is attached to a plate by using two independent mounting blocks as shown in figure 3.5. The base plate of the rolling road and the surroundings were painted with fluorescent paint so as to reduce reflection [34] as shown in figure 3.4

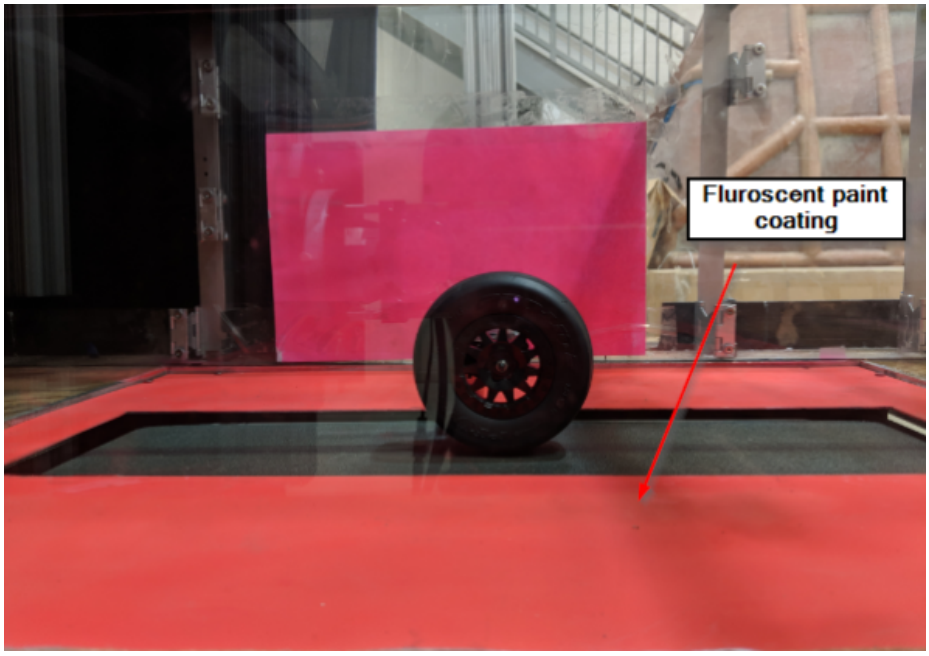

Figure 3.4: The tire assembly in the wind tunnel test section

Each of these mounting blocks have vertical bolt,which enable the vertical adjustment of the stinger relative to the ground i.e the rolling road as well as the ability to change the inclination angle. As it can be seen from the figure, each mounting block is again fitted with bolts perpendicular to the vertical bolts which can be used to adjust the position of the stinger in the x axis and also the slip angles. The experimentation was done for 0° inclination and slip angle.

Figure 3.5: The scaled tire assembly: slick tire attached to the tire mount

Since it is an open channel wind tunnel there are several parameters which affect the air intake and overall operation of the wind tunnel. Before an experimental run, the front portion of the wind tunnel is cleared of obstacles which would impact the flow intake into the wind tunnel. Due to the open channel nature of the wind tunnel, its operation is susceptible to change in temperature and pressure inside the research facility. The experimentation is done during early morning or late in the evening. This is done so as to minimize the impact of fluctuating temperature and pressure due to opening of the doors inside the Motorsports Research Center during daytime. The ventilation was also cutoff during the wind tunnel operation as an attempt to maintain an optimum/standard condition for the experimental run.

3.3 Camera

The camera used for conducting this study is a Dantec Flowsense 12M-70 able to capture full resolution double frame images at 25 Hz. The camera is equipped with a Nikon AF Nikkor 50 mm lens with an aperture size of f/8. The camera is also equipped with a long-pass filter of 532 nm to remove the background light leaving only the light fluoresced by the tracer particles. The camera is attached to an aluminum frame which is connected to the frame of the traverse on which the laser resides. This allows the simultaneous movement of the camera and the laser when the traverse is operated. This setup keeps the camera in focus with the area under investigation. The camera setup is made so as to capture the images on x-y plane keeping z constant.

3.4 Laser

The laser used for this study is a Litron LPY704-100 PIV Class IV (532nm) dual power, dual cavity, Nd:YAG with 12ns pulse width at 100 Hz. The laser has the capability to operate at 100 mJ per pulse. For this study the camera and the laser frequency were synchronized using a synchronizer (BNC) and is made to run a synchronized frequency of 25 Hz.

3.5 Seeding

For most of the experimental studies involving gaseous flows, a liquid seeding is used so as to reduce the density of the particles. Commonly used gaseous seeding particles are oil, Di-Ethyl-Hexyl-Sebacat (DEHS), smoke, and HFSB.

For gas flows, the increased density difference between the gaseous fluid medium and the particles can result in significant velocity lag as mentioned before in chapter 2. Solid particles, even if used, are very difficult to disperse into the gaseous medium and also have a tendency to agglomerate. For homogeneous seeding, the particles must be injected into the flow shortly before it enters the test section. The injection point for tracer particles should be done such that it does not interfere with the flow, but should ensure uniform seeding of the test section. For this the injection of tracer particles is done at the entrance of the Settling Chamber.

The test section is seeded with two different seedings. Part of this study compares the quality of seeding for the area under investigation using two different tracer particles, olive oil and Smoke.

3.5.1 Olive Oil Seeding

For most of the PIV measurements in gaseous flow, oil is used as the tracer particles and is dispersed using an atomizer. The advantages of using oil based seeding is its non toxic nature and do not vary in size significantly under various conditions.

The seeding generator consists of a cylindrical container with two air inlets and an aerosol outlet. Four pipes with valves mounted at the top of the container are dipped into an oil or similar liquid seeding material inside the container.These pipes are connected to one air inlet. These pipes are closed off at the ends. Four Laskin nozzles, 1 mm in diameter are equally distributed along the circumference of the pipes. A horizontal impactor plate is put inside the container so as to make small openings of around 2mm between the pipe wall and the inner wall of the impactor plate. There

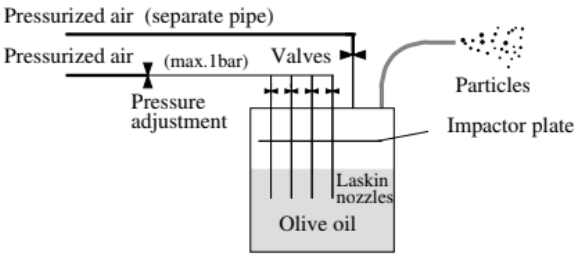

Fig. 2.9. Oil seeding generator.

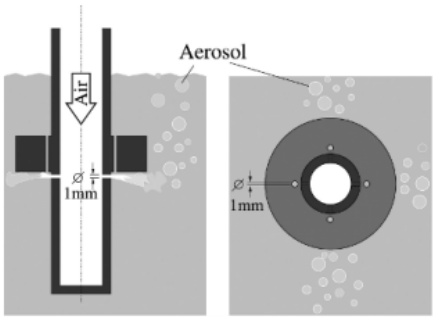

Fig. 2.10. Sketch of a Laskin nozzle.

Figure 3.6: Atomizer with laskin nozzle, Image credits: [32]

is also a second air inlet and an outlet which are connected at the top. The air is ejected as jets inside the liquid through the small 1mm nozzles using compressed air of 0.5 to 1 bar pressure. Due to the shear stress induced by these jets, small droplets are generated which are carried by the air bubbles to the top of the container and ejected through the aerosol outlet. The impacter plate functions as a sort of filter which filters out the bigger droplets from reaching the top of container and thus the outlet. The particle concentration can be decreased using the second air inlet.

The mean particle size depends primarily on the liquid which is atomized and slightly on the operating pressure of the atomizer. For this experiment, the atomizer was operated at 30 psi pressure. The seeding is discharged through an airfoil shaped rake which is made up of sequential holes along its leading edge as shown in the figure. The optimal seeding for a plane is obtained when the makeshift rake is tilted to roughly about 30°.

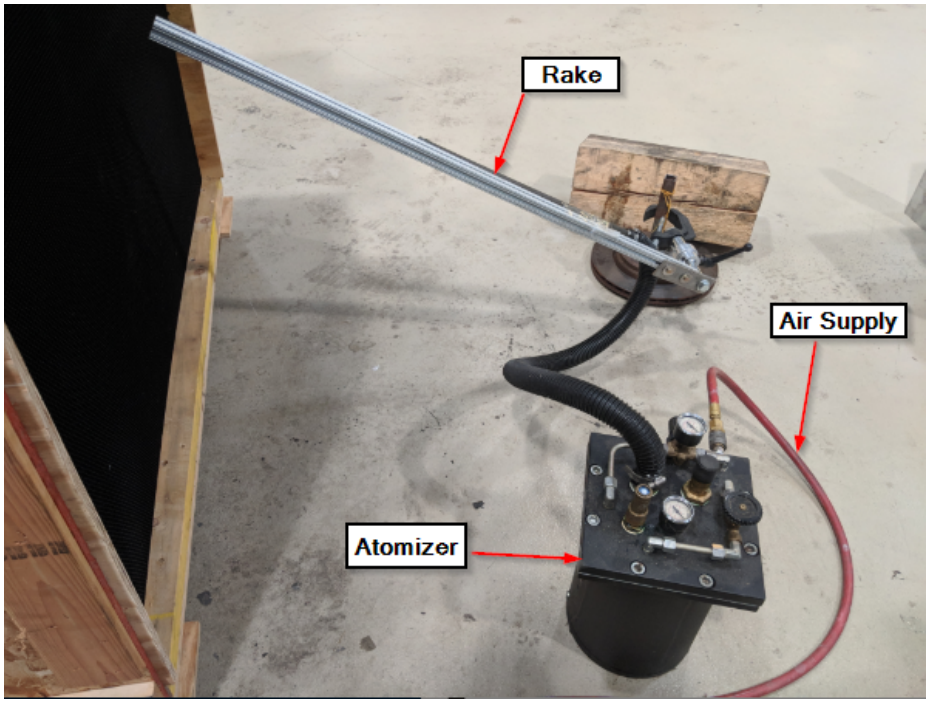

Figure 3.7: Olive oil seeding generator setup

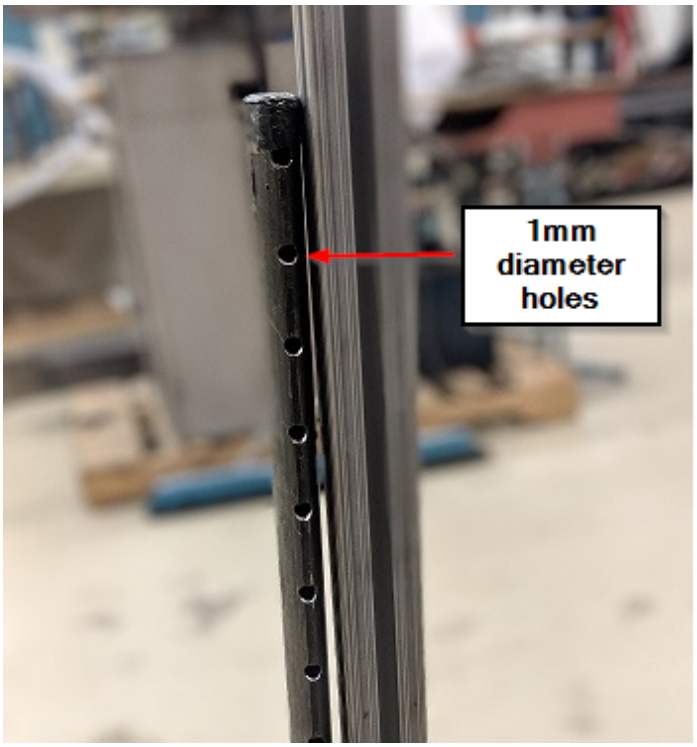

Figure 3.8: Olive oil rake closeup

3.5.2 Smoke Seeding

For smoke seeding, a smoke generator was used. The smoke was generated using a Rosco Vapor machine. A smoke fluid is used by the vapor machine to produce the smoke. The settings for the smoke generation are kept low for the PIV smoke run as shown in the figure 3.9

Figure 3.9: Smoke generator used for experimentation

3.6 Helium Filled Soap Bubble Seeding (HFSB)

The scattering efficiency of the tracer particles determine the field of view (FOV) for a PIV experimentation. Olive oil droplets or smoke particles typically have a diameter close to 1μm which limits the field of view. Alternatives to increase the FOV is to use a larger tracer particle. The increase the diameter of the particle enables better scattering efficiency. But increasing the size of seed/tracer particle also increases the density of the particles. Thus, these particles will not satisfy the neutrally buoyant condition needed for a tracer particle for PIV. A different approach to satisfy the neutrally buoyant condition for a tracer particle is by using helium filled soap bubbles. This technique thus offers a larger sized tracer particles but a lower density due to the presence of helium.

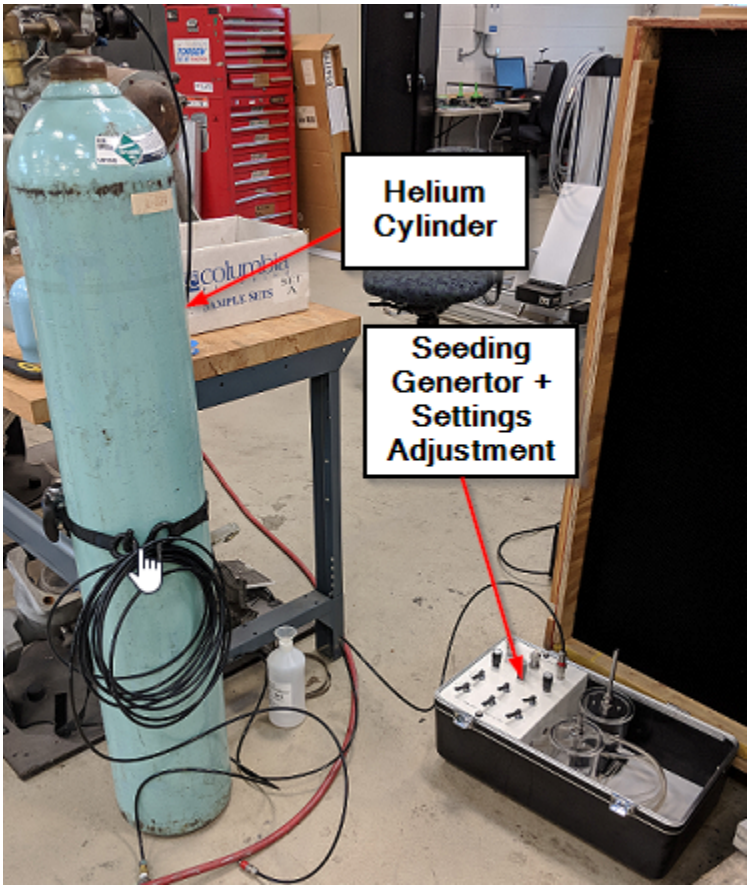

Figure 3.10: Helium Filled Soap Bubbles (HFSB) generator setup

Helium Filled Soap bubbles are generated by the apparatus as shown in 3.10. The soap solution is inserted into one of the openings as shown in the figure. The other ports are connected to an external air inlet and helium inlet from a helium tank. The small cyclone separator mixes the helium, air and soap bubbles evenly and separates the lighter particles from the denser particles and is these particles are channeled through the transparent tube and is directed towards the inlet of the wind tunnel.

3.7 Settling Chamber

The settling chamber is made up of layers of honeycomb and screens as shown in the figure 3.11. The main function of honeycomb is to reduce turbulence and to produce a consistent steady flow in the axial direction which is required for the test.

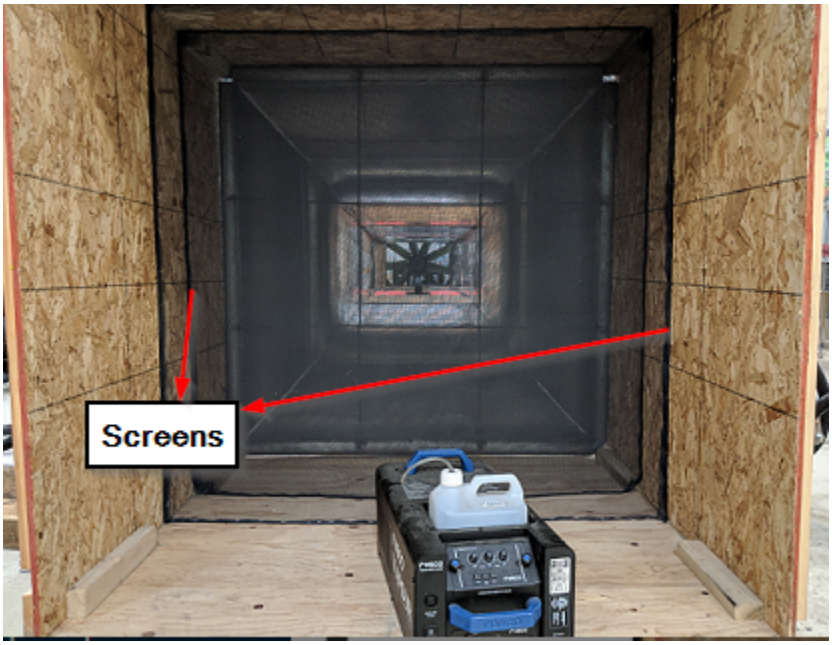

Figure 3.11: Inside of the settling chamber

The honeycomb is made up of hundreds of cells combined which are stacked together into a screen along the cross section of the settling chamber. These cells reduce the transverse velocity components of the flow with minimal pressure drop along the stream wise direction. This reduces the turbulent intensity at the inlet of the wind tunnel and thus for this study, provide uniform distribution of tracer particles along

the test section. The number of screens for the settling chamber depends on the flow quality required for the test. It is also to be noted that putting additional screens increases power requirement.

3.8 Calibration

The PIV system was calibrated using a 200mm × 200mm calibration target as shown in the figure below. The calibration target was placed perpendicular to the line of view of the camera and placed at the near end of the scaled tire. The calibration target is illuminated by a light source and the brightness of the image is calibrated by adjusting the f stop (focal length) of the camera.

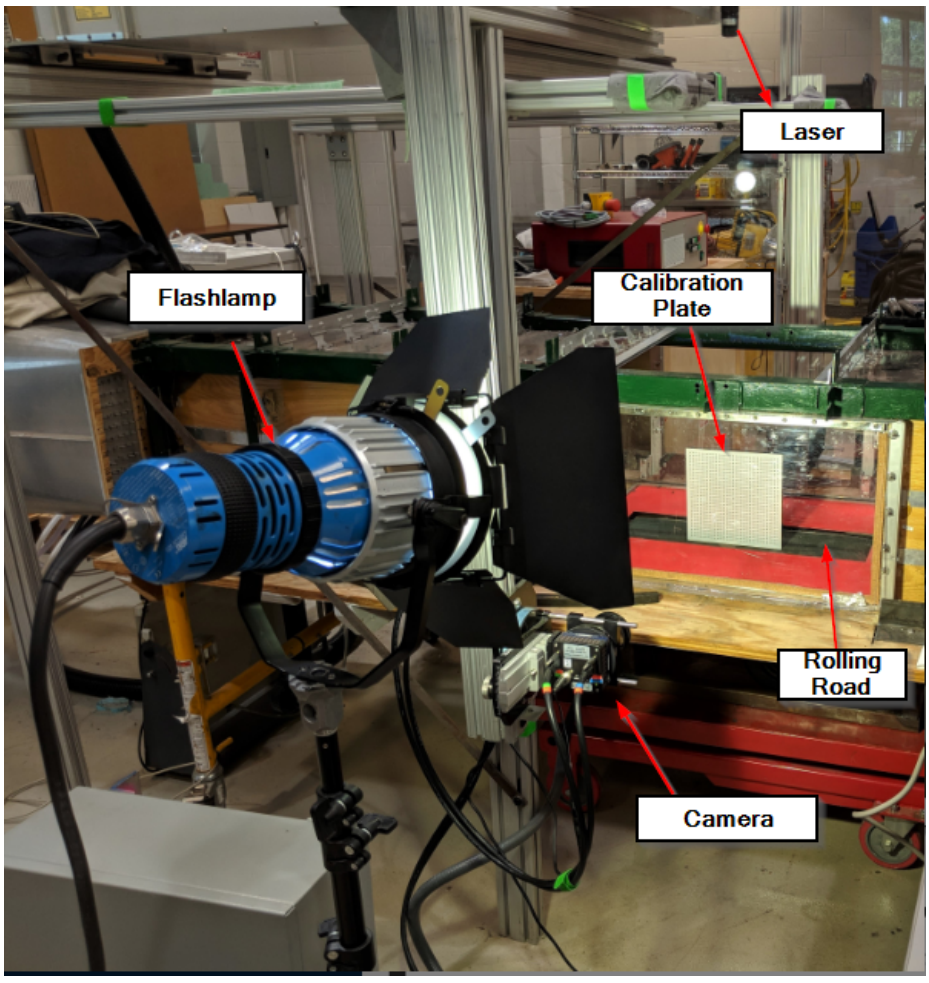

Figure 3.12: Calibration setup

The image being captured by the camera is refined for accuracy by manually ad-

justing the red dots between the image as shown in figure 3.13 below and entering the calibration length between them manually. The scaling data is automatically generated by the software. PIV software captures a calibration image which it uses for post processing of the captured data. The scaling ratio was automatically set to 12.85 pixels/mm.

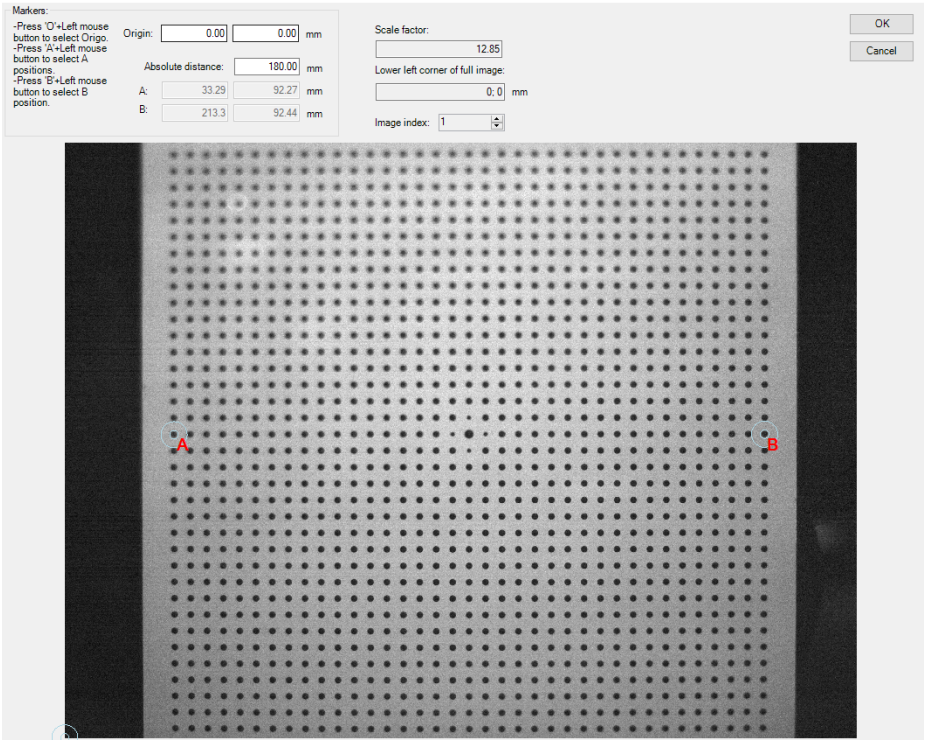

Figure 3.13: The calibration plate: 200 mm × 200 mm

3.9 Data Acquisition and Processing

The image was acquired and processing was done using Dantec Dynamics proprietary software DynamicStudio. The software synchronizes the camera and the laser to fire simultaneously.The synchronization is done with the help of a synchronization unit which triggers the laser and the camera. The acquisition hardware which includes the laser,traverse and the camera, hardware synchronization and data acquisition is integrated on the same workstation as that of the PIV software.

The image is acquired using acquisition manager module inside PIV software. The

acquisition manager controls several operational settings for the experiment. Acquisition manager controls the traverse movement in the x,y and z direction depending on whether its a 2-D plane experiment or 3-D. The software also dictates the time between pulses, trigger rate and the number of images per run. The images for the runs are captured in double frame mode. This allows the calculation of the velocity from the consecutive frames.

The processing was done using an Adaptive PIV algorithm which is proprietary to DynamicStudio software. The Adaptive PIV algorithm uses the principle of statistical cross correlation to analyze the raw images. The algorithm also adapts the interrogation area size according to number of tracer particles desired to be included in that area. The number of particles per interrogation area can be set as default or user defined. The method will iteratively adjust the size and shape of the individual interrogation areas (IA) in order to adapt to local seeding densities and flow gradients.

3.10 Empty Tunnel Testing and Processing

Prior to assessing the impact of various tracer particles on a rolling road-tire test setup, an empty tunnel testing with the tracer particles was done. This was done so as to narrow down the optimal tracer particle for the rolling road-tire experimentation between olive oil, smoke and HFSB. The empty tunnel testing also gives an idea of the seeding quality in the test section without any obstruction from a scaled model. The empty tunnel testing also gives the optimum settings for the seeding distribution and processing setup. This testing will also help to cut down on the processing time for evaluating the rolling road-tire experimentation by helping to choose the best performing tracer particles.

In this test, three types of tracer particles are studied in an empty channel to find the efficiency of the seeding before testing on the rolling road setup. The acquisition settings were set to capture 250 images per run. For the empty channel testing, just a single plane was analyzed so as to evaluate the performance of different seedings.

The tracer particles studied are smoke, olive oil and HFSB. The wind tunnel was run at 18 Hz frequency. This corresponds to a velocity of 11 m/s. The calibration was performed as discussed in the section 3.8.

3.11 Rolling Road-Tire Setup Testing and Processing

For the rolling road-tire setup the acquisition settings are kept as same as that for the empty channel testing. The camera was set to capture 250 images per run at 25 Hz. For the current test, the runs were done on multiple planes so as to get a good perspective for the flow around the tire. A traverse control was used to move the laser by fixed distance of 10mm for each consecutive plane.

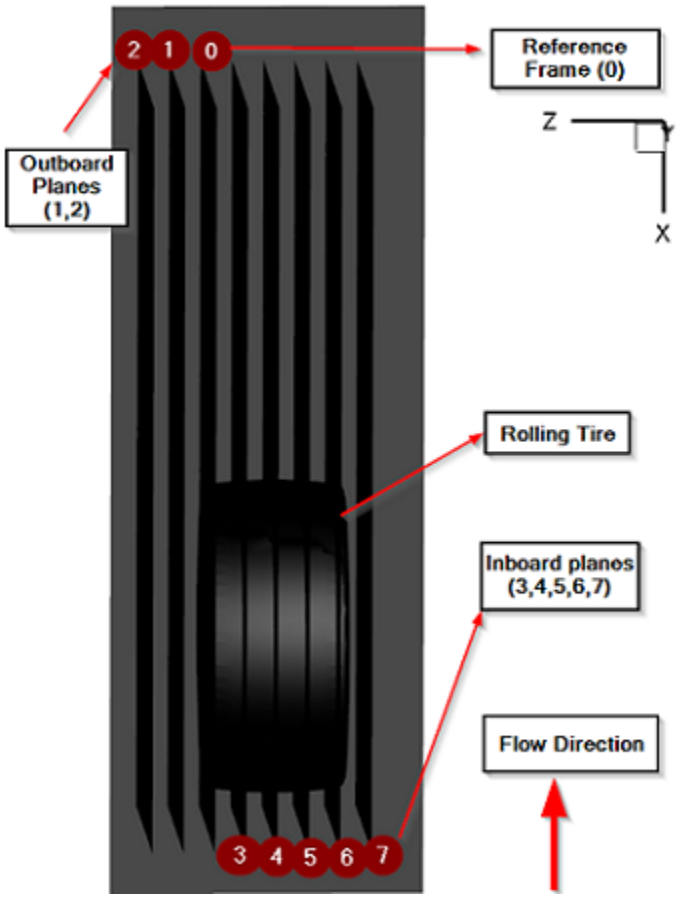

Figure 3.14: Cross sectional view of the planes studied - top view - 8 planes in 10 mm intervals

A total of 8 planes were studied starting from the 20mm outboard of the tire to 50

mm inboard of the tire. The planes are represented as shown in figures 3.14 and 3.15

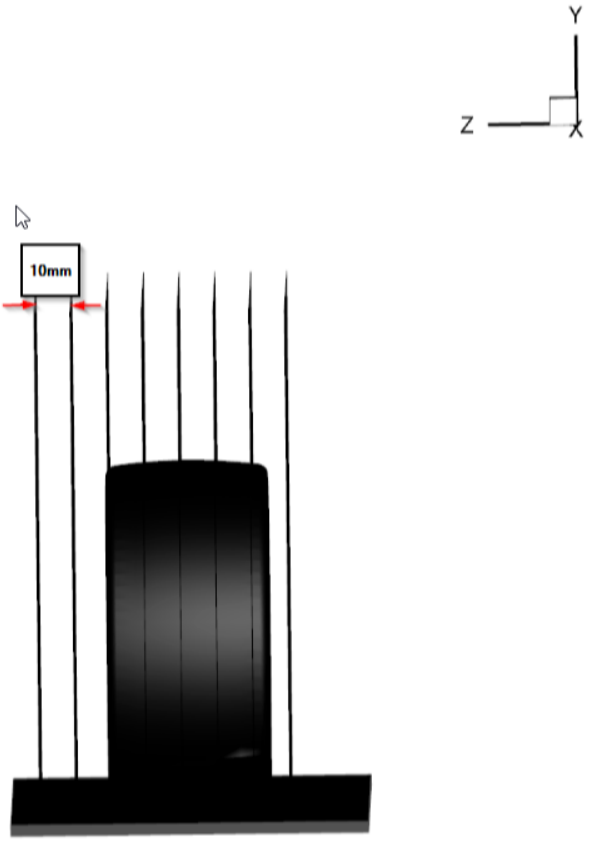

Figure 3.15: Cross sectional view of the planes studied - front view

The planes were analyzed using Adaptive PIV algorithm as mentioned in the Empty Channel Processing section. This Adaptive PIV algorithm is applied to all of 250 images captured per run for a plane. The Adaptive PIV algorithm creates a vector map of the instance using cross-correlation.

A single averaged vector map can be created from the 250 Adaptive PIV vector maps for a plane which gives a general idea about the flow for that plane over the tire. Subsequently averaged vector maps are created for the rest of the planes. For the planes encompassing the tire, a mask is defined so as to remove the incorrect data estimated by the software in place of the tire. The mask defined for processing is shown in the figure below 3.16

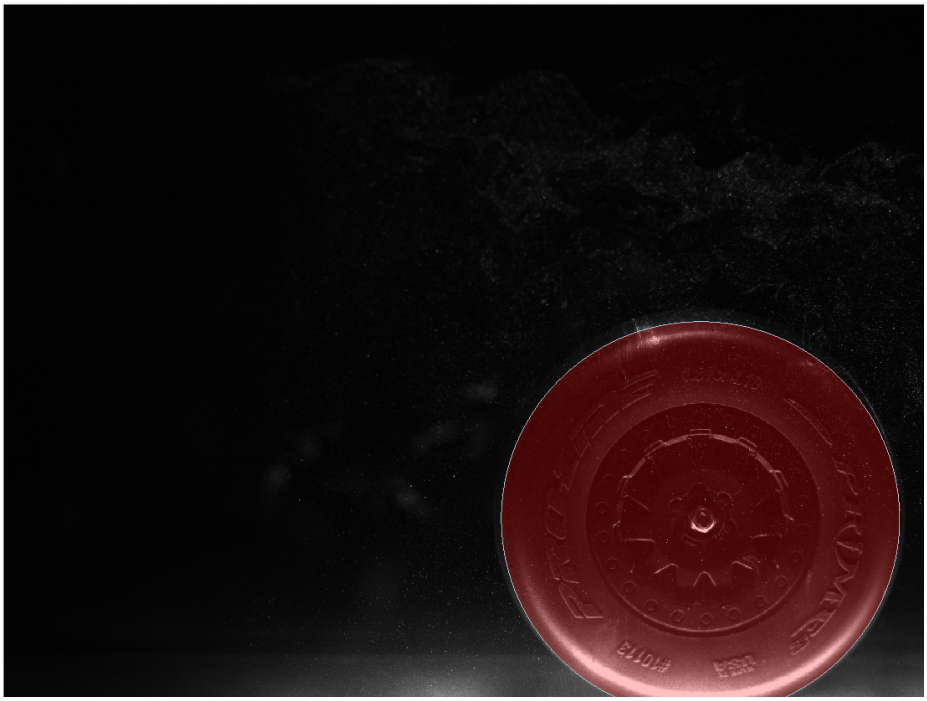

Figure 3.16: Tire mask defined in the software for post processing

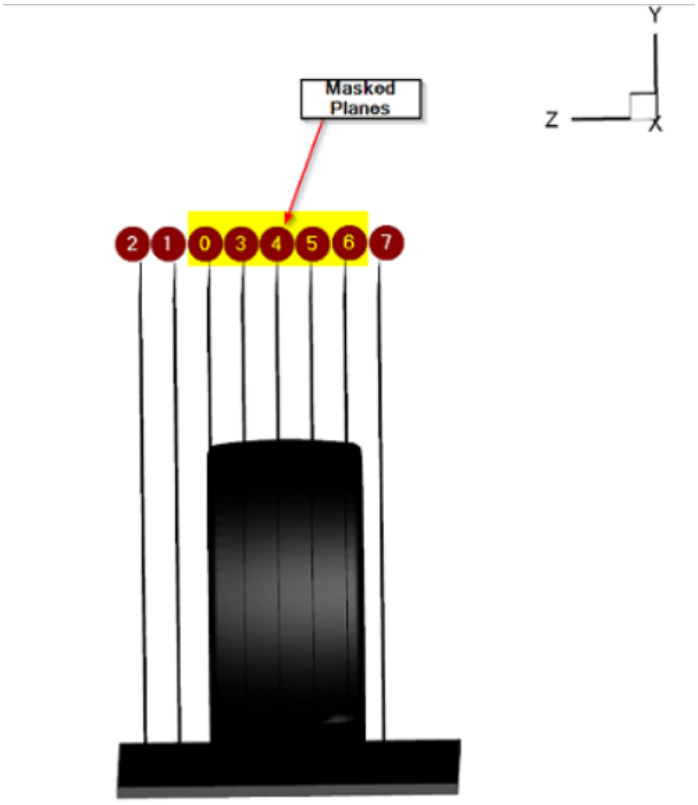

Figure 3.17: Masked planes

The mask are applied before processing the raw data using Adaptive PIV algorithm. The masks are applied to 0mm, 10mm, 20mm, 30mm and 40mm plane respectively to mask the tire.

The rolling road-tire setup was tested using olive oil and smoke seeding. For this testing HFSB seeding is omitted due to its poor performance as described in the Empty Channel Testing section. The experiment is conducted with similar settings to that for Empty Channel Testing. The camera f stop is set at f/8 for smoke testing and f/2.4 for olive oil testing. The image resolution was set to 4000 $\times$ 3000 pixels.

A calibration image is captured and the calibration procedure is exactly similar to that of Empty Channel Testing calibration. The calibration image is shown in figure 3.18 below.

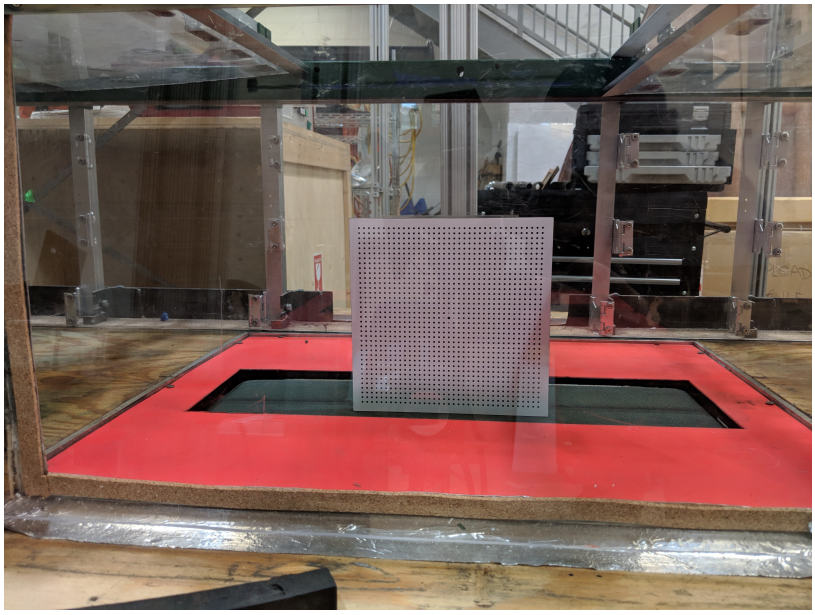

Figure 3.18: The calibration plate in the wind tunnel test section

For the Adaptive PIV algorithm, the grid step size was set to 16$\times$16, the minimum interrogation area size as 32$\times$32 and maximum interrogation area size as 64$\times$64. There was no filter applied for processing. For the PIV software settings, peak validation, the minimum accepted peak height, peak height ratio and the signal to noise ratios were set to 0.25, 1.15 and 4.0 respectively. For Universal Outlier Detection, the

neighborhood cells are kept to 5×5. It was not increased so as not to over analyze the raw data.

CHAPTER 4: RESULTS

4.0.1 Empty Tunnel Smoke Test Results

The smoke seeding was generated using a smoke generator with the lowest settings. The smoke generator produced a dense cloud of smoke that creates too much seeding for the test section under investigation. An over-saturated image is generated by the PIV software due to reflections created by this cloud of smoke. Due to this issue, the camera focal length is adjusted to reduce the reflection from the smoke particles. The camera focal length (f-stop) is adjusted to f/8, thus reducing the aperture and limiting the light intake into the camera. The time delay between consecutive images of a double frame image was altered by determining the required delay to track a single particle over a distance of ± 0.5 pixels. By visual inspection the time delay was found to be 70 μs.

The captured images were post processed and averaged. The average vector map generated for smoke seeding is as shown in figure 4.1 below. The flow is in turbulent regime test section.

$$R_e = \frac{vd}{\nu} = \frac{11m/s \times 0.3m}{1.57 \times 10^{-}5m^2/s} = 2.10 \times 10^5 \tag{4.1}$$

The seeding density was found to be 0.030 particles/pixel. From the average vector map, anomalies can be seen at the extreme edge of the vector map downstream of the flow. This inconsistency can be attributed to the configuration of the wind tunnel. Due to the changes made to the wind tunnel and the specific location of the laser with regards to the test section, the laser cannot reach the entire field of view and thus some information is lost downstream of the flow. The abnormality at the bottom of

the image can be attributed to the small turbulent boundary layers.

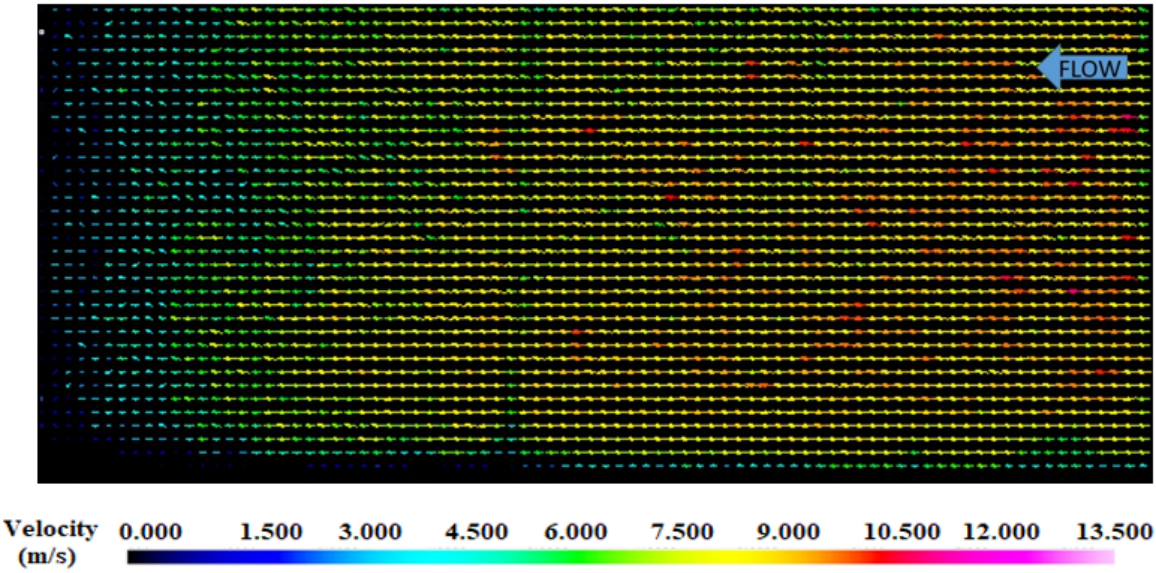

Figure 4.1: Average velocity vector map obtained from smoke seeding

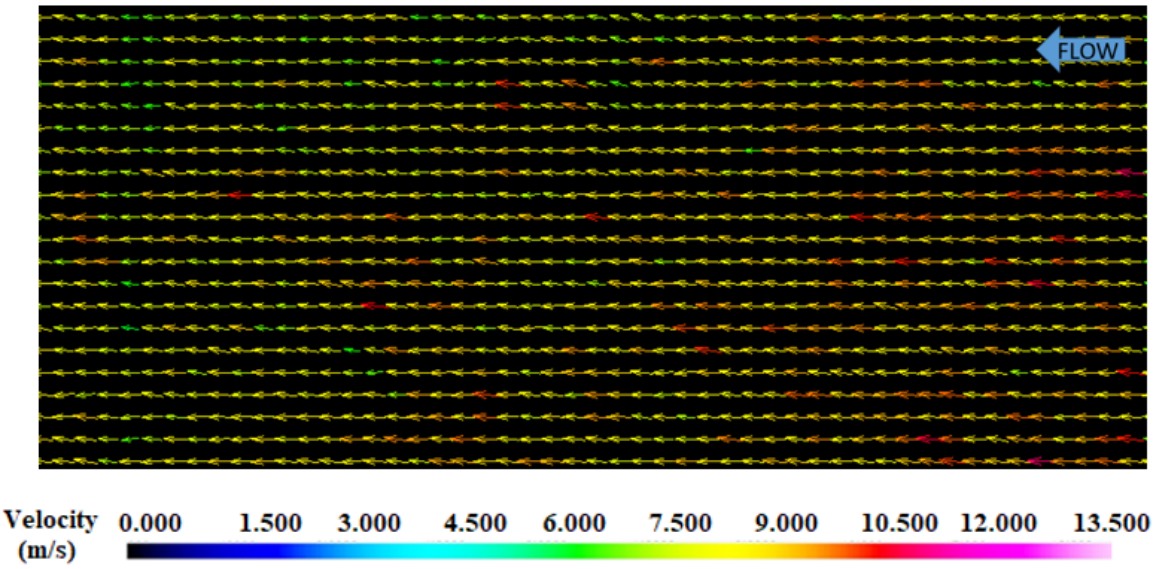

Figure 4.2: Closeup of the average velocity vector map obtained from olive oil from 4.1

It is also observed from the average vector map that the free stream velocity was less than that of the set velocity of the wind tunnel. This is further corroborated by the seeding distribution histogram, which indicates the velocity of around 48 percent

of the particles are in the range of 8-10m/s rather than the set wind tunnel speed of 11 m/s the sample data. Less than 5 percent of the particles are around 11 m/s. This considerable change could be attributed more to the pulsing action of the smoke generator than with the errors with the PIV system itself. The pulsing is caused when the smoke seeding generator, at its lowest setting, is unable to keep up with the wind speed of the tunnel. Due to this pulsing, the smoke seeding becomes inconsistent over the 250 images inside the test section, thus lowering the average velocity of the run.

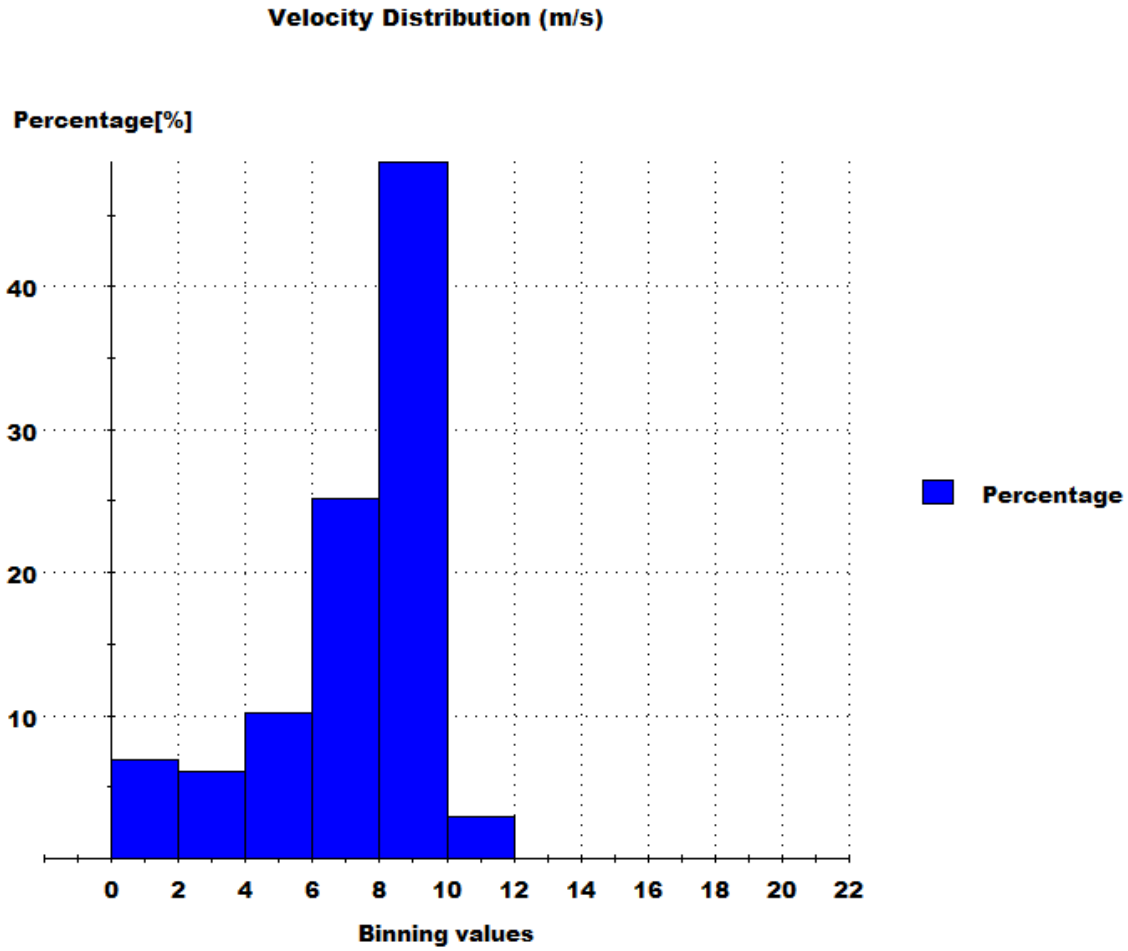

Figure 4.3: Velocity distribution of smoke seeding

4.0.2 Empty Tunnel Olive Oil Results

The olive oil was generated using an olive oil generator as discussed previously in subsection 3.5.1. The air intake for the olive oil generator is experimented with 20 psi and 30 psi pressure. The air intake is set at 30 psi to get a good consistent seeding in the test section. The olive oil generator produces few tracer particles compared to that of smoke; thus this avoids the problem of over saturation of the image due to particle reflections as in case of smoke. The focal length was adjusted to increase the light intake and thus the f stop was set at f/2.4 and the time delay for the consecutive images of the double frame was set at 70 μs.

The average vector map generated for olive oil seeding is as shown in figure 4.4 below.

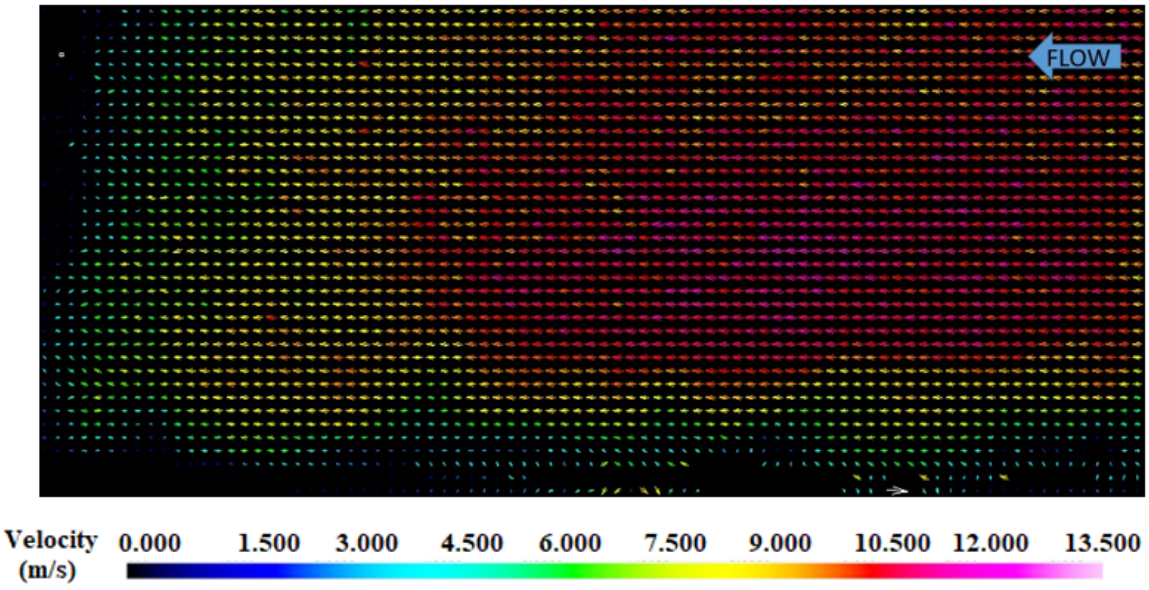

Figure 4.4: Average velocity vector map obtained from olive oil seeding

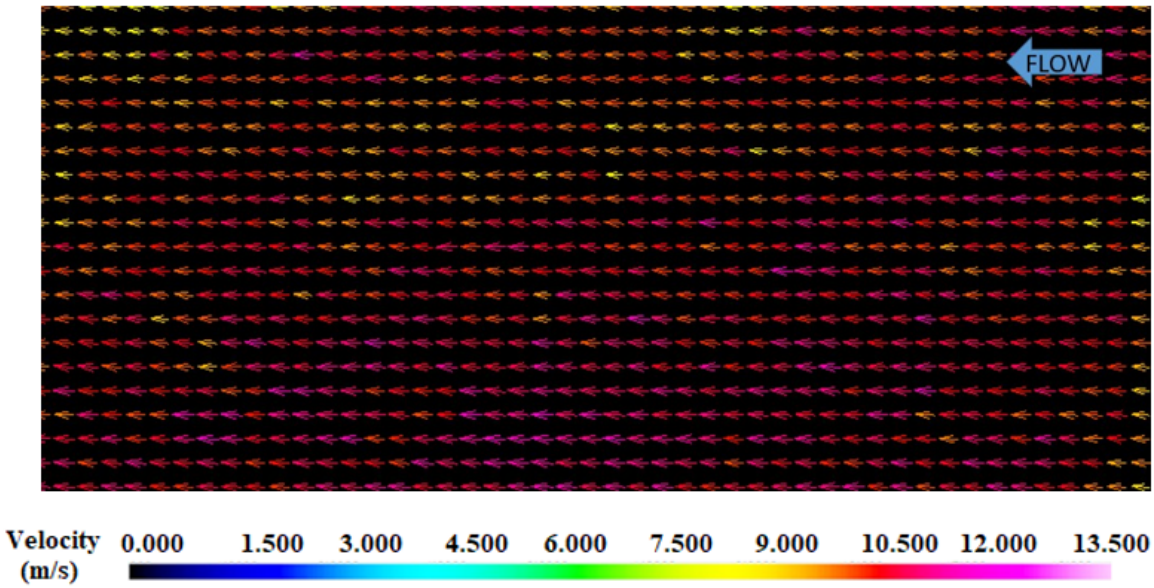

Figure 4.5: Close up of the average velocity vector map obtained from smoke seeding from 4.4

From the average vector maps from figure 4.4 and 4.5 it can be concluded that the flow is turbulent for the test section as in case of smoke, and there are abnormalities at the downstream as seen on the vector map due to similar reasons as explained with the smoke. The seeding density was found to be 0.035 particles/pixel. It was also observed that the olive oil seeding produces a consistent seeding when compared to smoke. The free stream velocity of olive oil seeding was found comparable to set wind tunnel speed. This could be attributed to the continuous supply of air intake which generates a consistent stream of tracer particles. The connection between the free stream velocity of an averaged vector map and the set speed of the wind tunnel can be further inferred from the velocity-seeding distribution histogram (Figure 4.6).

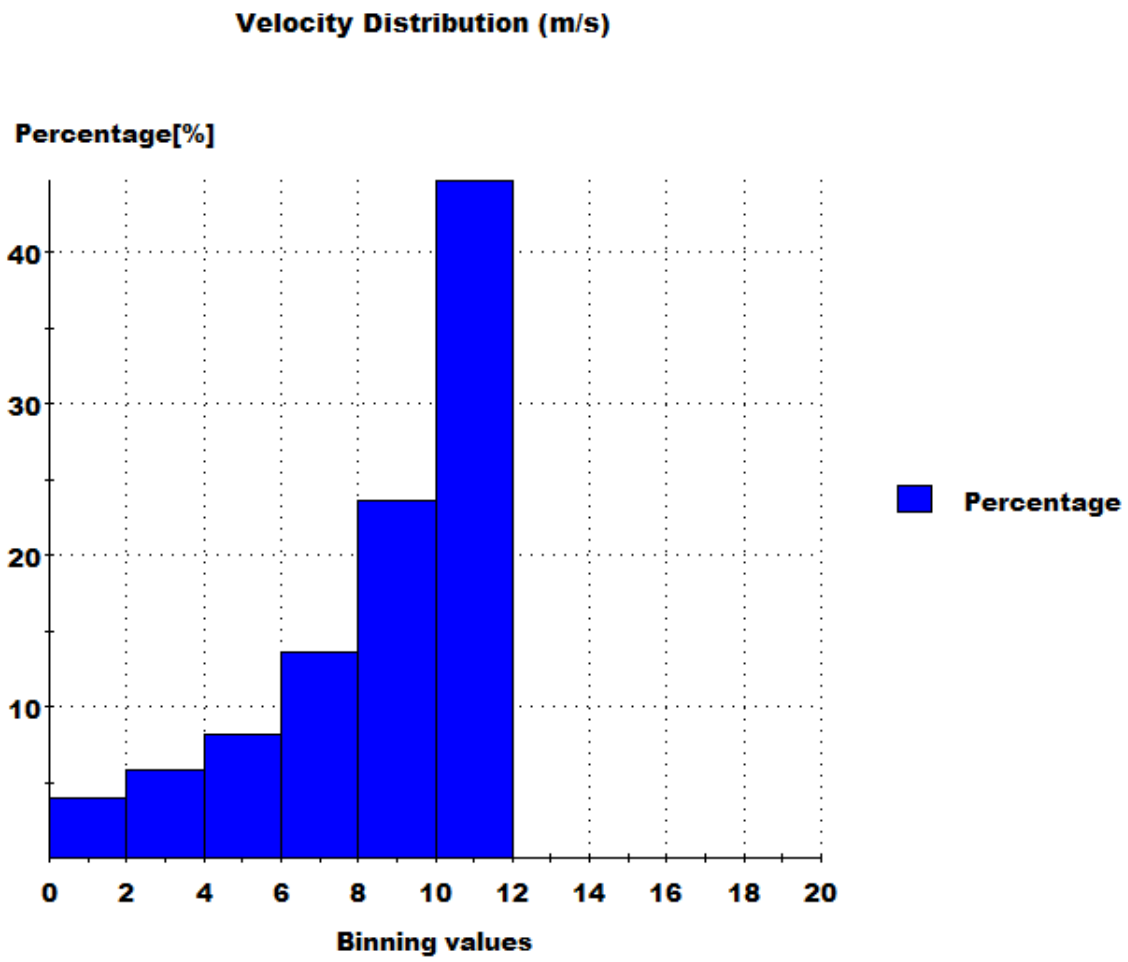

Figure 4.6: Velocity distribution of olive oil seeding

From the histogram it can be interpreted that around 45 percent of the olive oil tracer particles together have velocities ranging from 10-12 m/s, which is close to the wind tunnel speed set at 11 m/s.

4.0.3 Empty Tunnel Helium Filled Soap Bubbles Results

For HFSB testing, the seeding generation was done as discussed in subsection 3.6. The seeding generation was sparse compared to smoke and olive oil seeding. The focal length of the camera is set at f/2.4 since the density of the particles compared to smoke were minimal. The time delay for the run was set at 30 μs.

The HFSB seeding produces insignificant seeding which is unable to accurately track the flow. The seeding was tried to be improved upon by keeping the HFSB apparatus inside the settling chamber in between the honeycomb and the screens to minimize the seeding interference. Other settings were also altered to find the optimum seeding. The average seeding obtained is around 20-30 particles for the entire test section by visual inspection for a full run. The average seeding density was found to be 0.000 particles/pixel for the test section. The velocity of 30 percent of the sample data was found to be less than 1 percent as seen from the histogram in figure 4.7.

This kind of seeding is inconsequential and produced inaccurate results, thus the results from the HSFB can be invalidated. It was observed from the average vector map that the entire field seems to have a velocity that is completely random and does not have a particular direction like other tracer particles. It seems as if the vectors are diverging from certain points. This is a consequence of low seeding since the PIV software is unable to track any particles and tries to estimate the movements of the few known particles instead of tracking them. This estimation results in the unrealistic velocities in random directions.

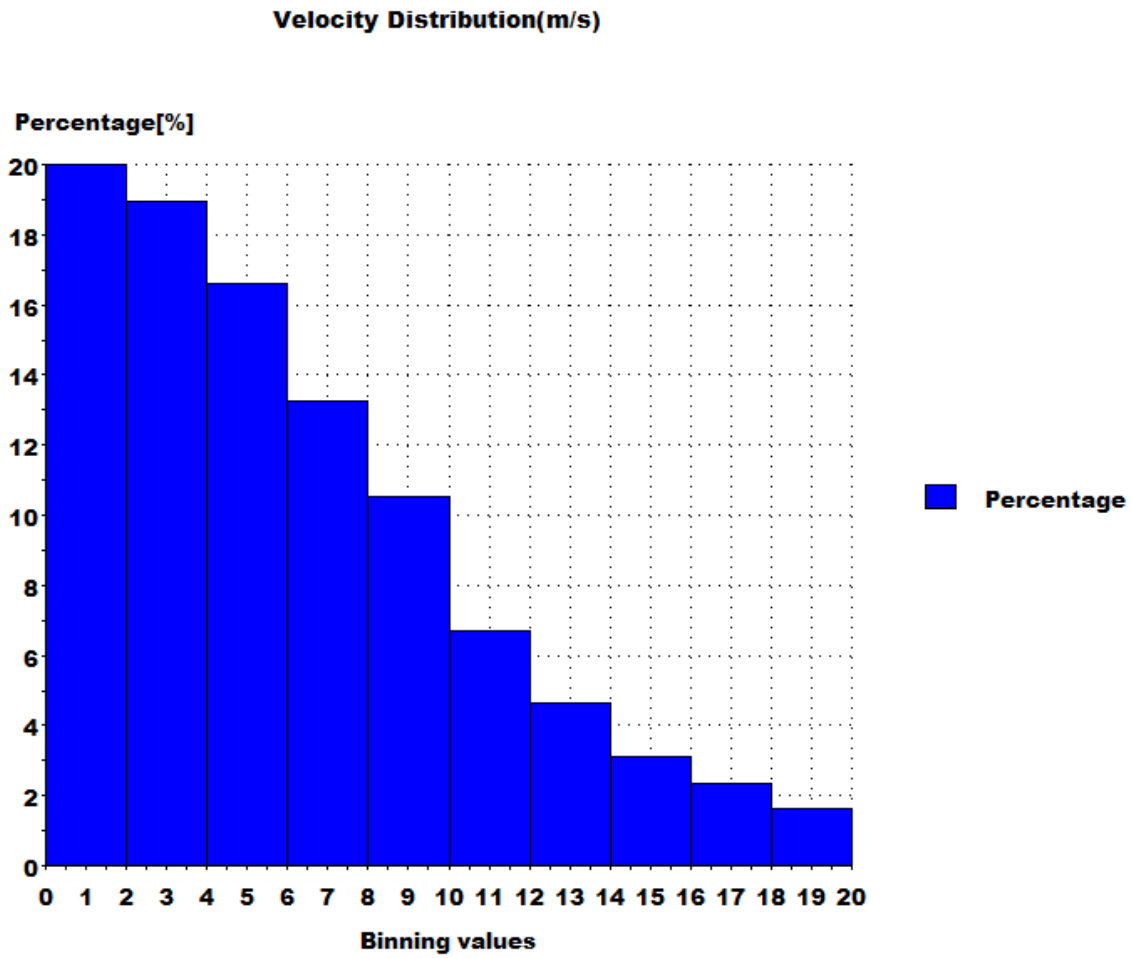

Figure 4.7: Velocity distribution of HFSB seeding

Due to inconclusive results from HFSB Empty Channel Testing, there was no further experimentation done with HFSB for rolling road-tire setup.

4.1 Rolling Road-Tire Setup Testing Results

For both the seeding, 250 images were captured per run for a total of 8 planes with an interval of 10mm. The captured planes are two outboard planes of 20mm and 10mm, one reference origin plane at 0mm, and five inboard planes at 10m, 20mm, 30mm, 40mm and 50mm. For post processing, the Adaptive PIV algorithm was running for each of these planes to obtain an instantaneous vector map for that particular image. The upper regions of the area under study was omitted due to poor seeding. This would help to decrease the processing time as well as remove the false vectors created during post processing of this sparse seeding. Similarly, all of 250 raw camera images are processed and their instantaneous vectors created. The instantaneous vectors only give a general idea of the flow for that instance. In the efforts to analyze the flow, these instantaneous vector maps are averaged using Vector Statistics algorithm in PIV software.

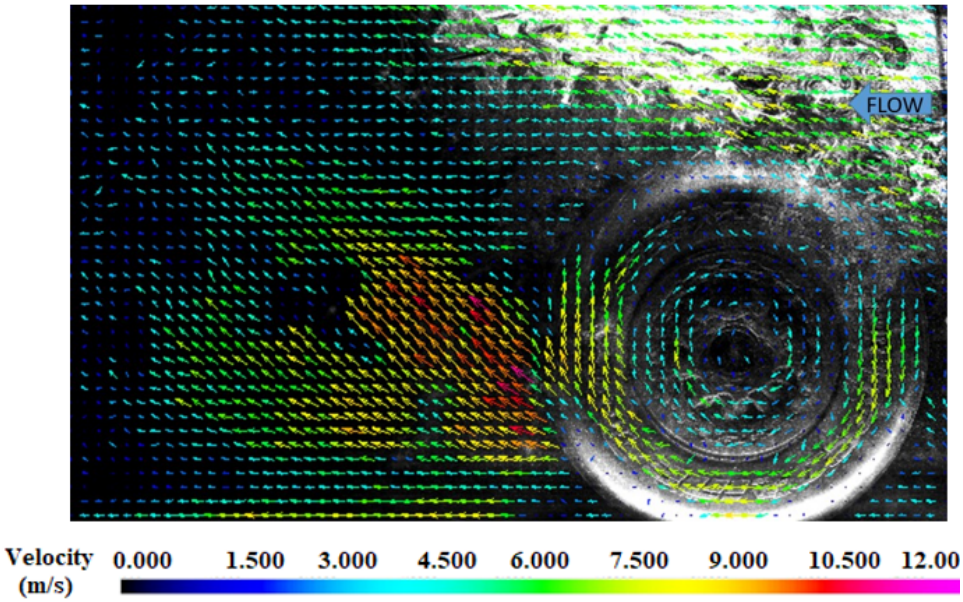

Figure 4.8: Smoke vector statistics data layered with one of the raw images for 10mm outboard plane

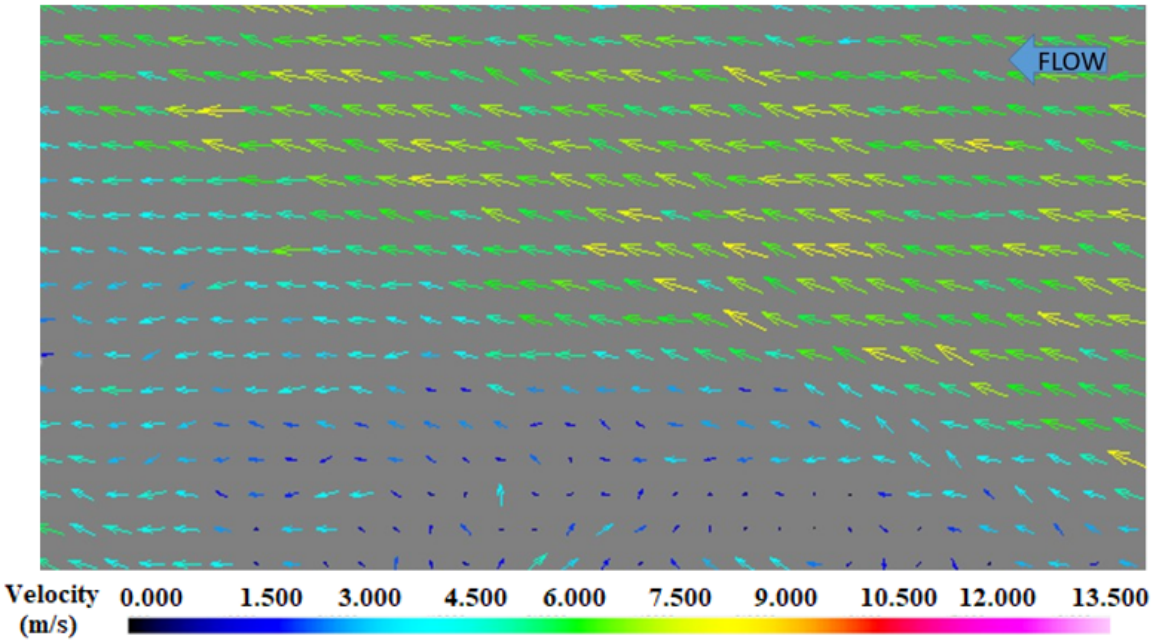

Figure 4.9: Close up image of the smoke vector statistics data of figure 4.8

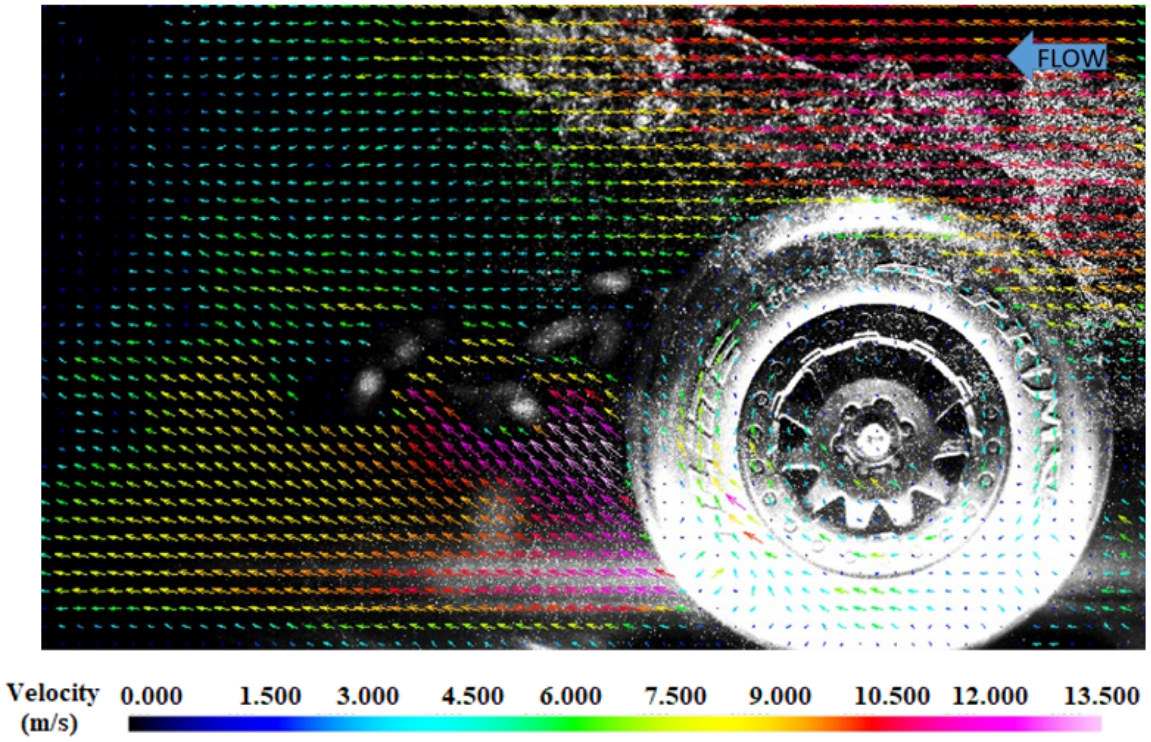

Figure 4.10: Olive oil vector statistics data layered with one of the raw images for 10mm outboard plane

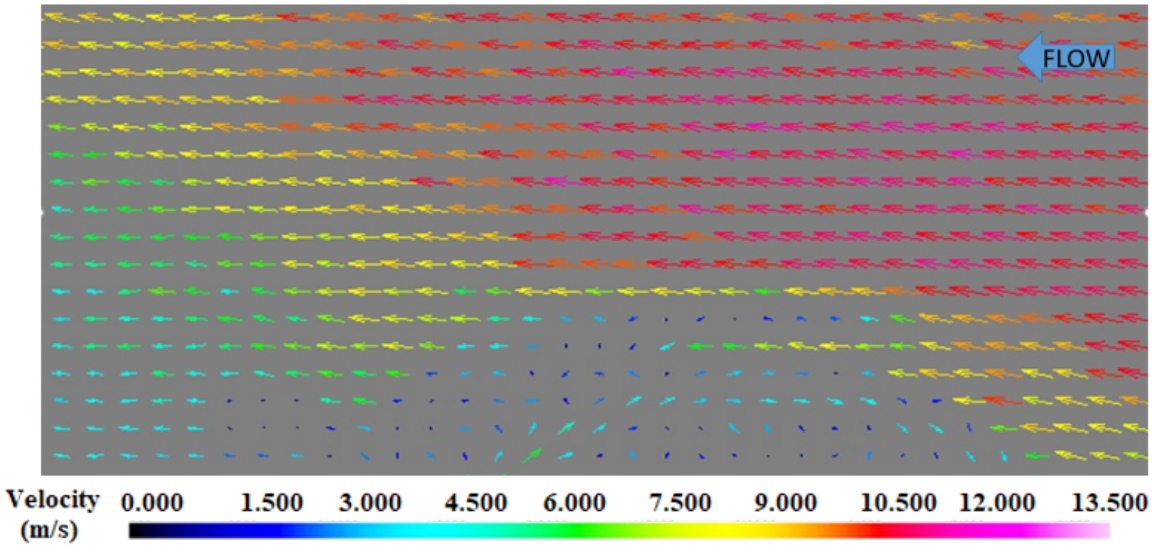

Figure 4.11: Close up image of the olive oil vector statistics data of figure 4.10

From the averaged vector maps of both the seedings as shown in figures 4.8, 4.9, 4.10 4.11 and , it can be observed that the free stream velocity for smoke seeding is less than that of set free stream velocity of 11 m/s. Thus this phenomenon of lower free stream velocity than set wind tunnel velocity result is similar if not exact to that obtained during Empty Tunnel Testing. For the olive oil seeding, it has a free stream velocity comparable to that of the set wind tunnel velocity.

The olive oil was found not exhibiting a similar anomaly as that with smoke seeding. This is further validated by olive oil seeding results from the Empty Tunnel Testing. Thus this difference could be narrowed down to the method used for dispersal of tracer particles into the wind tunnel provided the other conditions are kept the same. An obvious argument which can be made is that of the pulsing action of smoke generator during its discharge of tracer particles into the wind tunnel. Even though time interval of this pulsing action is small enough, it could cause a non uniform seeding over time for the area under investigation and the averaging of these instantaneous velocity vectors for the complete run could alter the average free stream velocity.

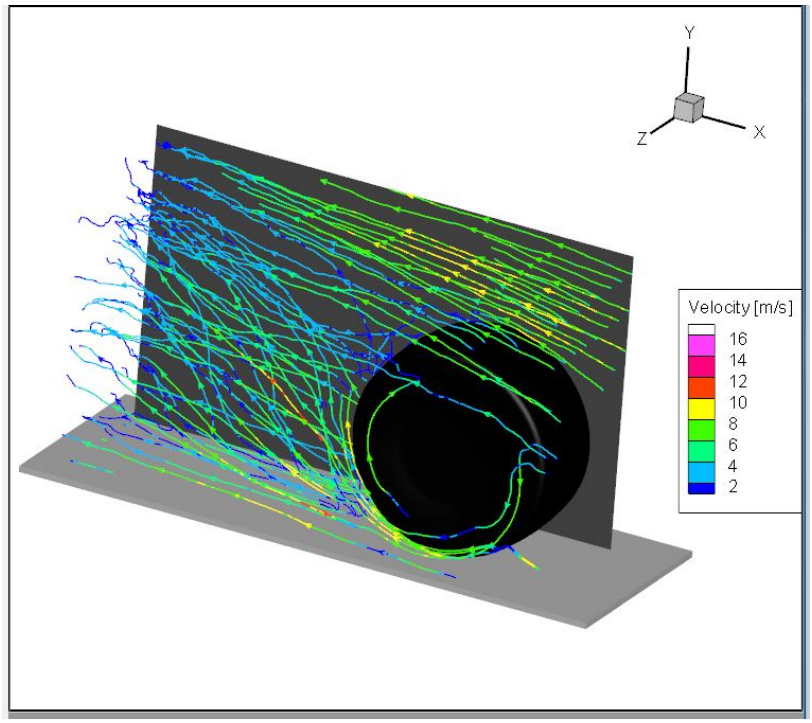

Figure 4.12: Smoke velocity vector data from post processing using Tecplot

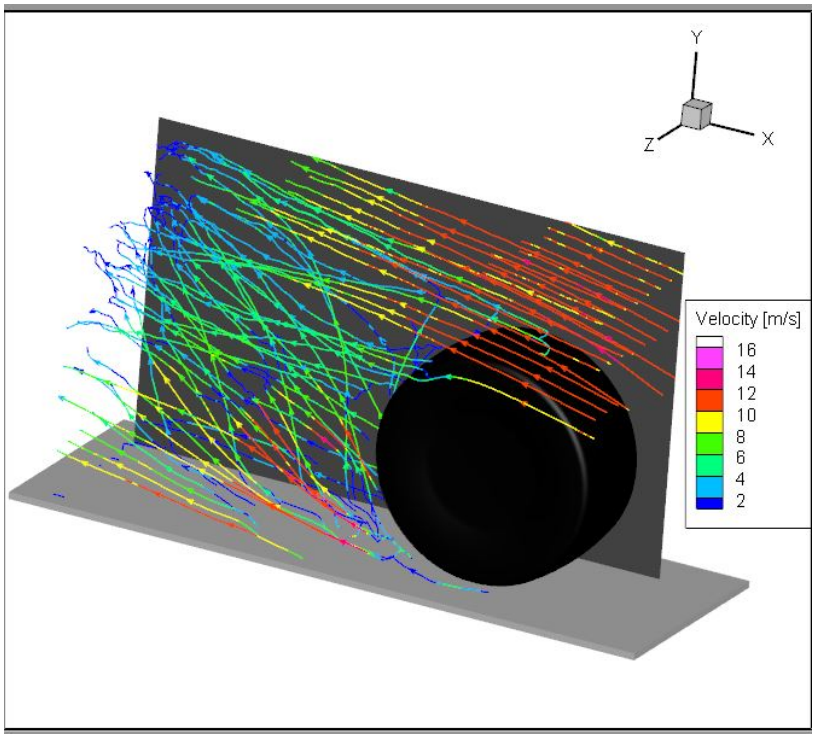

Figure 4.13: Olive oil velocity vector data from post processing using Tecplot

There also appears to be a vortex formation at the outboard of the tire in case

of smoke seeding which is absent in case of olive oil seeding. At first this vortex formation was assumed to develop due to the hub of the tire.

But on further investigation it can be argued that these vortex formation takes place due to reflection of tire brand inscription and this being captured by the PIV software as particle movement.

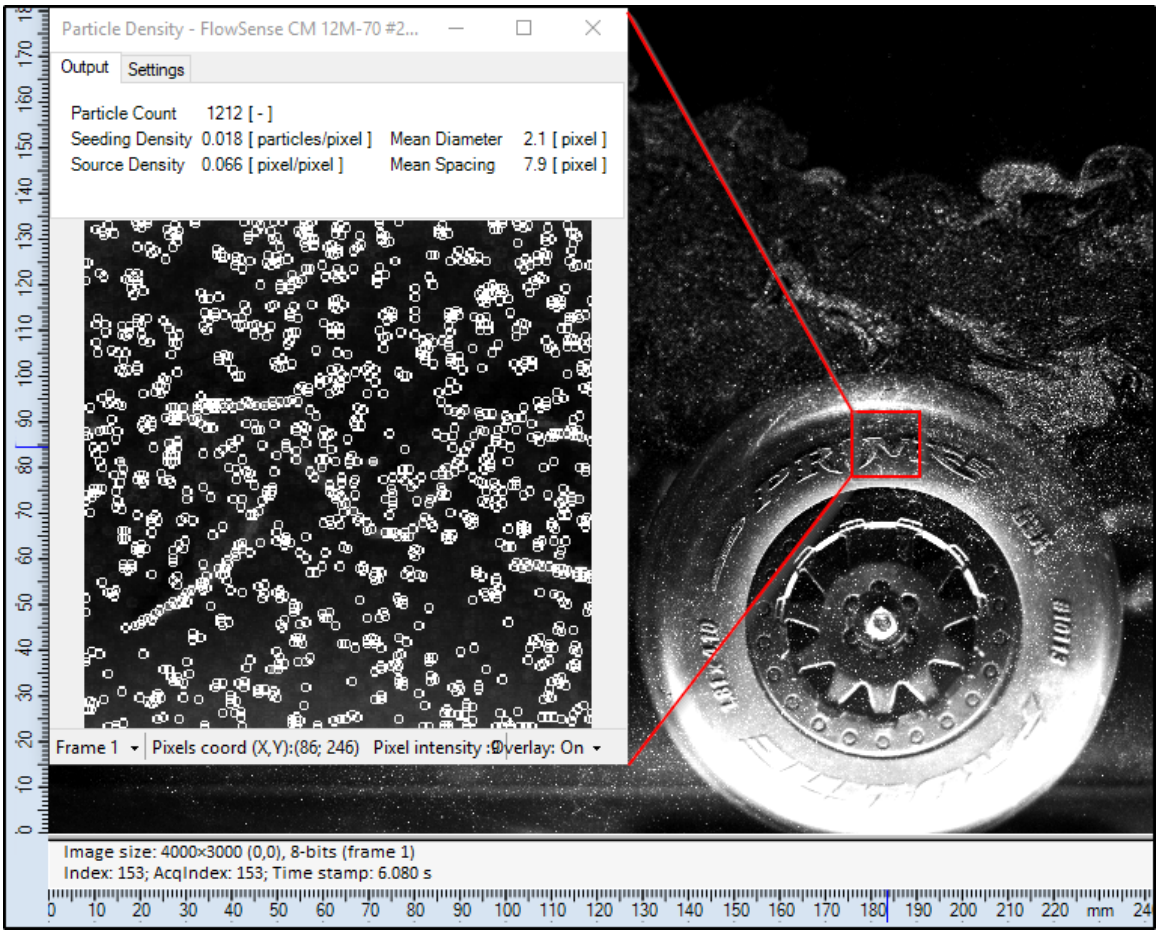

Figure 4.14: Particle density for one of the olive oil seeding runs

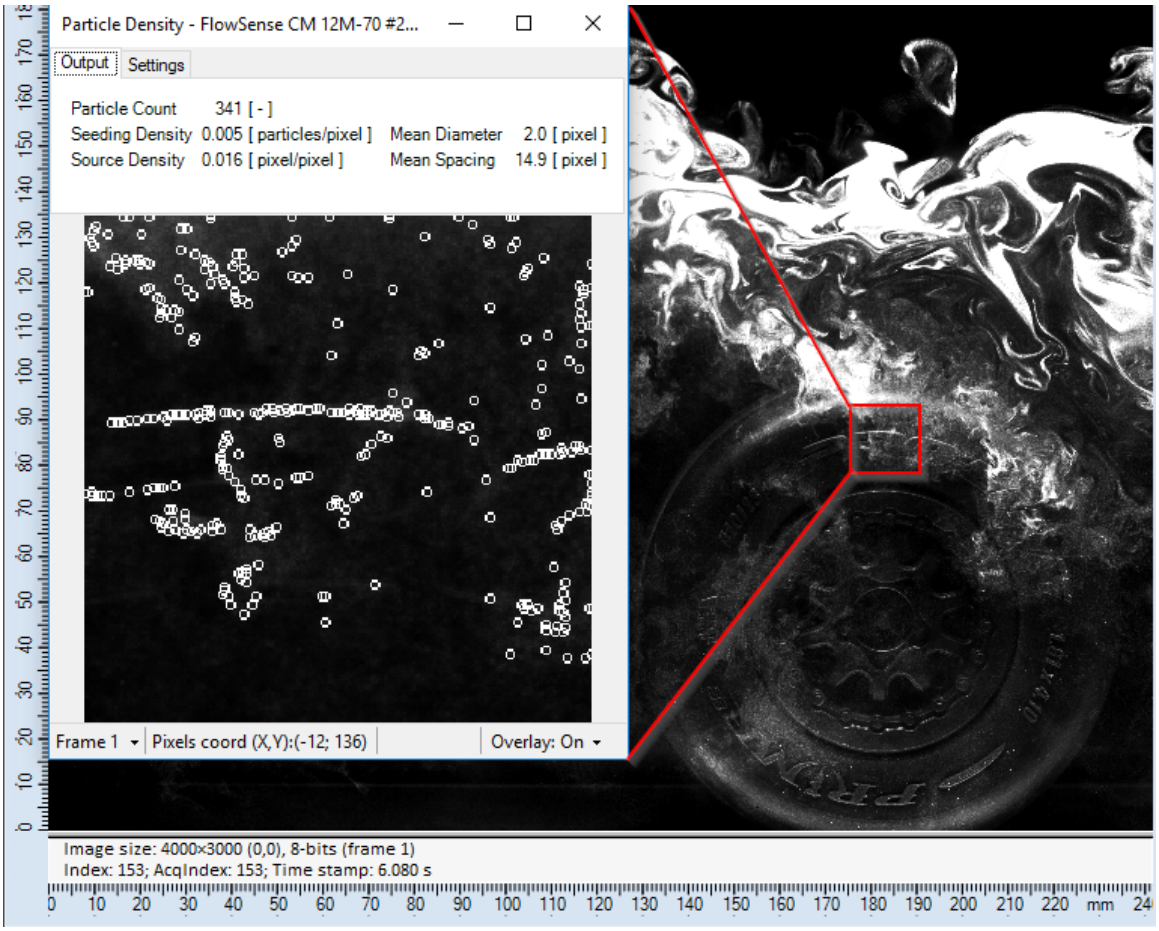

Figure 4.15: Particle density for one of the smoke seeding runs

By analyzing the raw instantaneous images for the outboard runs for both the seedings from the figures 4.14 and 4.15, it can be seen that the seeding for smoke was inconsistent near the tire. Due to this inconsistent seeding and also due to over saturation of this inconsistent smoke seeding, the number of particles being visualized by the PIV software is low when compared to the particle count obtained from olive oil seeding for the same instance.

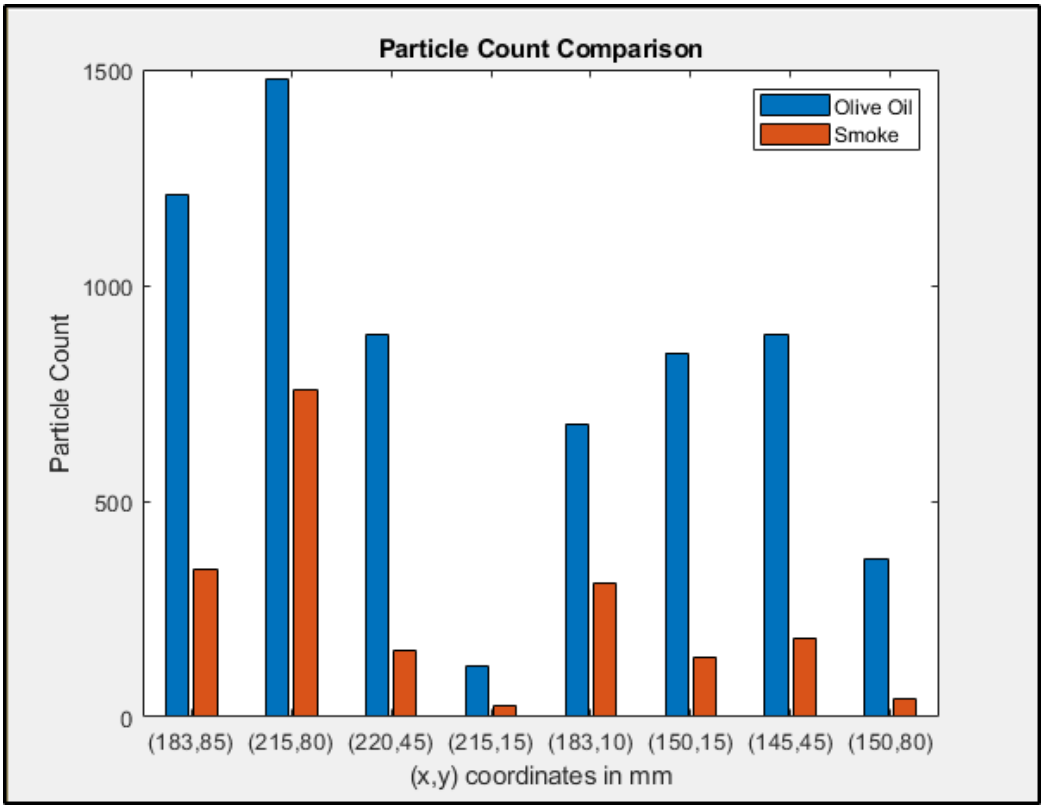

Figure 4.16: Particle count comparison of the tracer particles along the circumference of tire from one of the instantaneous vector maps for 10mm outboard runs

The figure 4.16 gives a histogram for the particle count from one of the instantaneous images out of the 250 images around the tire for outboard 10mm plane. The coordinates on the x axis describes the points selected along the circumference of the tire for evaluating the particle count and the y axis describes the particle count. A total of 8 points were selected for visualization. As can be visualized from this histogram, the particle count for olive oil is relatively higher when compared with smoke seeding. This trend of the increased olive oil particle count continues throughout almost all the instantaneous images for both the 10mm and 20mm outboard planes.

It could assumed that, due to inconsistent seeding across the tire , there are not enough data points in the images for the sofware to process. This inconsistent tracking of reflection of particles combined with the tire rotation causes the false tracking by the PIV software. Since the tire is rolling throughout a particular run, this misinterpreted

particle movement data creeps into the average vector map which shows up as vortex formation outboard of the tire. In the case of olive oil particles there were enough particles to completely discern the flow direction and thus the software was able to accurately track the particles across the tire.

Both the seedings struggle with replicating the flow at the edge of the downstream test area as can be seen from at left most edge of figures 4.8 and 4.10. This could be attributed to the distribution of the laser, more precisely the laser beam not illuminating the rear end of the investigation area downstream sufficiently. This again can be attributed to the wind tunnel configuration. It should also be noted that the current result would not be possible if the rolling tire is replaced with a static tire for the test configuration.

CHAPTER 5: CONCLUSION

The aim of this work was to compare the accuracy of multiple tracer particle types in visualizing flow over a scaled tire on a rolling road inside a small scale wind tunnel via PIV. The rolling road-tire experimentation was performed using a 1/10th scaled tire and analyzed with an Nd:YAG laser in conjunction with a sCMOS camera and commercial PIV software. A settling chamber was added to smooth out the entrance flow to the test section. Initially, all the tracer particles were studied for an empty test section to evaluate the consistency of particle seeding. For this work, only a single plane was evaluated. From the empty wind tunnel testing, HFSB tracer particle type was eliminated due to its inconsistent seeding in the test section. Comparing olive oil and smoke, it was determined that olive oil tracer particles allow higher resolution images for yielding PIV flow parametric data such as vortex formation and free stream velocity. More specifically, the average velocity of smoke was comparatively less than that of the olive oil. One of the reasons for this difference occurring could be due to the pulsing action of the smoke generator in the experiments. Inconsistency could also be due to a combination of operating factors such as the operating temperature and pressure. From this research, it can be concluded that olive oil seeding is more suitable than smoke for PIV analyses of rolling road-tire experiments. Future work should incorporate a pre-mixing chamber in front of the settling chamber to release the tracer particles in the test section uniformly (even particle dispersions).

REFERENCES

[1] A. Melling, "Tracer particles and seeding for particle image velocimetry," *Measurement Science and Technology*, vol. 8, no. 12, p. 1406, 1997.

[2] A. K. Prasad, "Particle image velocimetry," *CURRENT SCIENCE-BANGALORE-*, vol. 79, no. 1, pp. 51–60, 2000.

[3] P. Bryanston-Cross and A. Epstein, "The application of sub-micron particle visualisation for piv (particle image velocimetry) at transonic and supersonic speeds," *Progress in Aerospace Sciences*, vol. 27, no. 3, pp. 237–265, 1990.

[4] R. Höcker and J. Kompenhans, "Application of particle image velocimetry to transonic flows," in *Applications of Laser Techniques to Fluid Mechanics*, pp. 415–434, Springer, 1991.

[5] M. Molezzi and J. Dutton, "Application of particle image velocimetry in high-speed separated flows," *AIAA journal*, vol. 31, no. 3, pp. 438–446, 1993.

[6] C. Towers, P. Bryanston-Cross, and T. Judge, "Application of particle image velocimetry to large-scale transonic wind tunnels," *Optics & Laser Technology*, vol. 23, no. 5, pp. 289–295, 1991.

[7] W. Humphreys, S. Bartram, and J. Blackshire, "A survey of particle image velocimetry applications in langley aerospace facilities," in *31st Aerospace Sciences Meeting*, p. 411, 1993.

[8] R. D. Keane and R. J. Adrian, "Optimization of particle image velocimeters. i. double pulsed systems," *Measurement science and technology*, vol. 1, no. 11, p. 1202, 1990.

[9] W. W. Hunter Jr and C. Nichols Jr, "Wind tunnel seeding systems for laser velocimeters," 1985.

[10] C. Kähler, B. Sammler, and J. Kompenhans, "Generation and control of particle size distributions for optical velocity measurement techniques in fluid mechanics," *Exp Fluids*, vol. 33, pp. 736–742, 2002.

[11] C. Kähler, "General design and operating rules for seeding atomisers," in *5th International Symposium on Particle Image Velocimetry*, 2003.

[12] A. Melling, "Seeding gas flows for laser anemometry," tech. rep., CRANFIELD INST OF TECH (ENGLAND) SCHOOL OF MECHANICAL ENGINEERING, 1986.

[13] P. Tkacik, Z. Carpenter, A. Gholston, B. J. Cobb, S. Kennedy, E. Blankenship, M. Uddin, and S. P. Krishna Nukala, "A low cost rolling road for tire measurements in a small eiffel wind tunnel," in *SAE World Congress Experience, WCX 2017, April 4, 2017 - April 6, 2017*.

[14] A. Morelli, "Aerodynamic actions on an automobile wheel," in *Road Vehicle Aerodynamics, Proceedings of the First Symposium on Road Vehicle Aerodynamics, City University, London, edited by AJ Scibor-Rylski*, 1970.

[15] W. Stapleford and G. Carr, *Aerodynamic characteristics of exposed rotating wheels*. Motor Industry Research Association, 1969.

[16] A. Cogotti, "Aerodynamic characteristics of car wheels," *INT. J. VEHICLE DESIGN- IMPACT AERODYNAMICS ON VEHICLE DESIGN, 1983*, pp. 173–196, 1983.

[17] J. E. Fackrell, *The aerodynamics of an isolated wheel rotating in contact with the ground*. Thesis, 1974.

[18] J. Fackrell and J. Harvey, "The flow field and pressure distribution of an isolated road wheel, advances in road vehicle aerodynamics," in *BHRA Fluid Engineering Conference-Paper*, vol. 10.

[19] L. Axon, K. Garry, and J. Howell, "An evaluation of cfd for modelling the flow around stationary and rotating isolated wheels," Report 0148-7191, SAE Technical Paper, 1998.

[20] P. Bearman, D. De Beer, E. Hamidy, and J. Harvey, "The effect of a moving floor on wind-tunnel simulation of road vehicles," Report 0148-7191, SAE Technical Paper, 1988.

[21] E. Mercker and H. Berneburg, "On the simulation of road driving of a passenger car in a wind tunnel using a moving belt and rotating wheels," in *Congresso ATA, Innovation and Reliability in Automotive Design and Testing, Firenze, Italy*.

[22] M. Hinson, "Measurement of the lift produced by an isolated, rotating formula one wheel using a new pressure measurement system," *Master's Thesis, Cranfield University*, 1999.

[23] A. P. Mears and R. G. Dominy, "Racing car wheel aerodynamics - comparisons between experimental and cfd derived flow-field data," in *Motorsports Engineering Conference and Exhibition, November 30, 2004 - December 3, 2004*, SAE Technical Papers, SAE International.

[24] A. Wäschle, S. Cyr, T. Kuthada, and J. Wiedemann, "Flow around an isolated wheel-experimental and numerical comparison of two cfd codes," tech. rep., SAE Technical Paper, 2004.

[25] A. Mears, S. Crossland, and R. Dominy, "An investigation into the flow-field about an exposed racing wheel," Report 0148-7191, SAE Technical Paper, 2004.

[26] A. J. Saddington, R. D. Knowles, and K. Knowles, "Laser doppler anemometry measurements in the near-wake of an isolated formula one wheel," *Experiments in Fluids*, vol. 42, no. 5, p. 671, 2007.

[27] R. D. Knowles, "Monoposto racecar wheel aerodynamics: investigation of near-wake structure and support-sting interference," 2007.

[28] J. Axerio, G. Iaccarino, E. Issakhanian, K. Lo, C. Elkins, and J. Eaton, "Computational and experimental investigation of the flow structure and vortex dynamics in the wake of a formula 1 tire," Report 0148-7191, SAE Technical Paper, 2009.

[29] A. J. Sprot, D. B. Sims-Williams, and R. G. Dominy, "The aerodynamic characteristics of a fully deformable formula one wind tunnel tyre," *SAE International Journal of Passenger Cars - Mechanical Systems*, vol. 5, no. 2, pp. 1026–1041, 2012.

[30] E. Issakhanian, C. J. Elkins, L. Kin Pong, and J. K. Eaton, "An experimental study of the flow around a formula one racing car tire," *Journal of Fluids Engineering*, vol. 132, no. 7, p. 071103 (8 pp.), 2010.

[31] M. Hamdi, M. Havet, O. Rouaud, and D. Tarlet, "Comparison of different tracers for piv measurements in ehd airflow," *Experiments in fluids*, vol. 55, no. 4, p. 1702, 2014.

[32] M. Raffel, C. E. Willert, F. Scarano, C. J. Kähler, S. T. Wereley, and J. Kompenhans, *Particle image velocimetry: a practical guide*. Springer, 2018.

[33] J. L. Dahlberg, *Aspects of Turbulence and Stochastic Processes in Fluid Mechanics*. PhD thesis, University of North Carolina at Charlotte, 2018.

[34] T. T. Bisel, J. L. Dahlberg, T. R. Martin, S. S. Owen, R. G. Keanini, P. T. Tkacik, N. Narayan, and N. Goudarzi, "A comparison of flat white aerosol and rhodamine (r6g) fluorescent paints and their effect on the results of tomographic piv measurements," in *ASME 2017 International Mechanical Engineering Congress and Exposition*, pp. V007T09A018–V007T09A018, American Society of Mechanical Engineers, 2017.

APPENDIX A: CHALLENGES

The were several challenges encountered during this research study.

1. The wind tunnel had to be restructured with lexan sheets so as to get a transparent test section area for the PIV testing. Other small scale maintenances had to be done in order for the wind tunnel to be ready for testing. Also an 80 x 20 frame was built over the wind tunnel to support the laser and the traverse.

2. The rolling road frame was eliminated so as to fit the rolling road setup at the base of the test section. An aluminum sheet with a cutout for the rolling road was attached to the base. This aluminium sheet was painted with fluorescent paint so as to minimize the reflection from the laser as stated by TT Bisel et.al.[34]. This aluminium sheet sits flush with the rolling road thus reducing interference for the free stream flow in the experiment.

3. After experimenting with different native seeding configurations, it was concluded that there was a need for a settling chamber which would smoothen out the turbulent eddys in the flow. A settling chamber was built with the help of Dr.Jerry Dahlberg which was attached to the inlet of the wind tunnel.

4. Since it is an open return wind tunnel, the surrounding conditions affect its operation. Even though careful considerations were made to keep the operating conditions constant, any fluctuation of these conditions, unknown to the author could impact the final result.

5. For this particular laser setup in small scale wind tunnel at UNC Charlotte Motorsports, the laser system broke down after calibrating individual laser to different laser energy levels. The flash-lamp of the lasers had to replaced twice during this research. So it is advised not to alter the individual energy levels for further experimentation.